

Chapter 6

Socioeconomic and Environmental Changes in Global Drylands



Shilong Piao, Yangjian Zhang, Zaichun Zhu, Xu Lian, Ke Huang,
Mingzhu He, Chuang Zhao, and Dan Liu

Abstract Drylands are a pivotal component of Earth's biosphere and provide essential ecosystem services to mankind. Over the past several decades, with rapid population growth, global drylands have been experiencing quick socioeconomic transitioning. Such socioeconomic changes, together with fast climate change, have dramatically altered dryland ecosystem functioning and the quality and quantity of ecosystem services they provide. In fact, complex interactions among climate, vegetation, and humans, involving multiple biophysical, biogeochemical, societal, and economic factors, have all played important roles in shaping the changes in global dryland environment. A comprehensive review of socioeconomic and environmental changes of global drylands and their underlying mechanisms would provide crucial knowledge informing ecosystem management and socio-ecological capacity buildup for a more sustainable future of global drylands. In this chapter, we would begin with summarizing the characteristics of socioeconomic changes in drylands. We then presented and discussed past and future projected changes in dryland ecosystem structure and functioning (e.g., vegetation growth, land cover changes,

S. Piao (✉) · X. Lian · M. He
Sino-French Institute for Earth System Science, College of Urban and Environmental Sciences,
Peking University, Beijing 100871, China
e-mail: slpiao@pku.edu.cn

S. Piao · D. Liu
State Key Laboratory of Tibetan Plateau Earth System, Resources and Environment (TPESRE),
Institute of Tibetan Plateau Research, Chinese Academy of Sciences, Beijing 100101, China

Y. Zhang · K. Huang
Institute of Geographic Sciences and Natural Resources Research, Chinese Academy of Sciences,
Beijing 100101, China

Z. Zhu
School of Urban Planning and Design, Peking University Shenzhen Graduate School, Peking
University, Shenzhen 518055, Guangdong, China

C. Zhao
College of Resources and Environmental Sciences, China Agricultural University,
Beijing 100193, China

© The Author(s) 2024

B. Fu and M. Stafford-Smith (eds.), *Dryland Social-Ecological Systems in Changing Environments*, https://doi.org/10.1007/978-981-99-9375-8_6

carbon sink, water-use efficiency, resistance/resilience to disturbances) and hydrological cycles (e.g., soil moisture, runoff, and groundwater storage). We also discussed new understandings of mechanisms underlying dryland eco-hydrological changes.

Keywords Dryland ecosystems · Gross primary productivity · Land cover change · Crop yields · Carbon–water coupling · Hydrology · Socioeconomic changes · Vulnerability

6.1 Changes of the Socioeconomic System in Drylands

6.1.1 *Human Population and Its Regional Variation*

Among the 7.3 billion (in 2015) people in the world, 2.56 billion lived in drylands (Fig. 6.1). A striking characteristic of the global population distribution is strong spatial unevenness at the continental scale (Fig. 6.2). In Sub-Saharan Africa, South Africa, and West Asia, over 75% of the population is distributed in their dryland part. In countries like Mexico, Peru, Bolivia, and Australia, this proportion typically exceeds 50%. Generally, human populations in drylands are more sparsely distributed than those in non-dryland systems at the national scale. As of 2015, more than half of the human population living in drylands was located in African countries (Fig. 6.1). The 10 countries with the most densely populated drylands in the world are located in Africa (Ethiopia, South Africa, Burkina Faso, and Morocco), Asia (India, Iran, China, Turkey, and Afghanistan), and North America (Mexico). It is predicted that the human populations in drylands in Turkey, Iran, China, and Burkina Faso will double by 2050.

6.1.2 *Net-Migration in Dryland Regions*

Net population migration (immigration minus emigration) is indirectly estimated as the difference between population change and natural population growth. Hotspots of negative net migration from drylands, indicating population loss due to migration, are found in Asia (Pakistan, Syria, Iran, and Uzbekistan), Africa (Nigeria, Somalia, and Morocco) and South America (northeast Brazil) (Fig. 6.3). Migration losses may be driven by environmental factors, such as increased drought frequency, severe heat-waves, or other extreme climate events, and by non-environmental factors such as land degradation or limited technological resources (Neumann et al. 2015). Hotspots of positive net migration into drylands, indicating population growth due to migration, are found in the United States, Zimbabwe, India, and China, with a total net

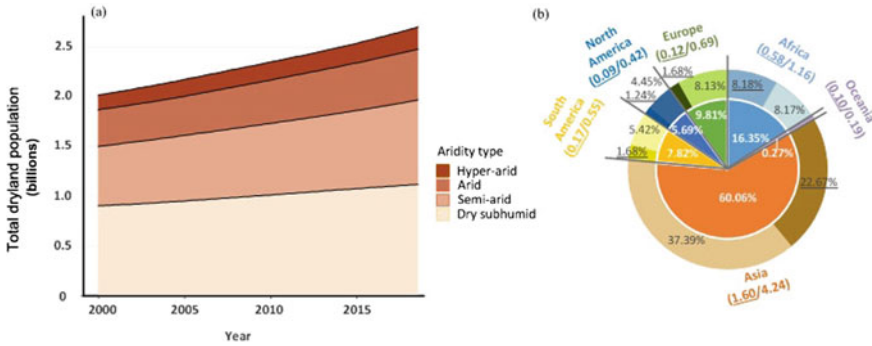


Fig. 6.1 **a** Changes in the human population in dryland regions of different aridity levels, over 2000–2018. **b** Percentages of continental populations living in drylands in 2015. Numbers below each continent label represent the population in billions. Numbers in the inner pie chart indicate the percentage of the global total, and those over the outer ring indicate the proportion of the continental population living in drylands and non-drylands. Underlined values represent drylands

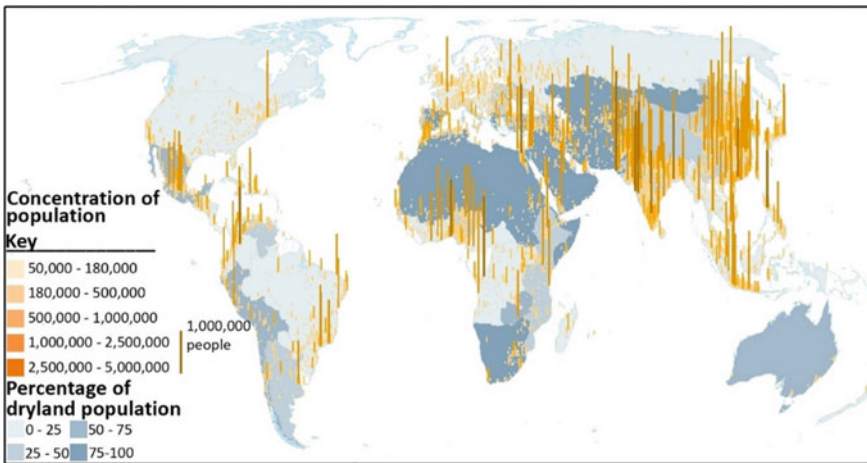


Fig. 6.2 Global distribution of human population in 2015. Areas with <50,000 individuals per cell (10×10 km) are not shown. Bar heights reflect population size

gain of over 100 million people. Countries with positive net migration generally have greater and more varied employment opportunities, higher incomes, more developed technology, and stronger government policies aimed at sustainable land development.

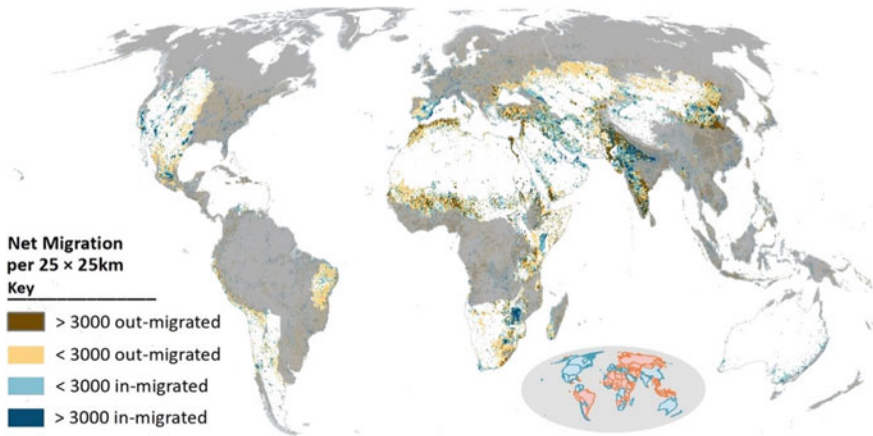


Fig. 6.3 Global pattern of net migration during 2010–2015. Dark gray shading indicates humid regions. The inset panel shows countries with net emigration in pink, and countries with net immigration in blue. Countries without drylands are not shown

6.1.3 Projected Population Growth

The Shared Socioeconomic Pathways database suggests that the global population in drylands will peak by the 2060s and then undergo a slight decline, leading to an overall increase of 25% by the end of the century (Fig. 6.4). During 2010–2050, the human population in drylands will increase by an estimated 1.1 billion people; 47% of this increase will be contributed by Africa (0.52 billion) and 34% (0.36 billion) by Asia, with smaller increases projected for North America (0.09), South America (0.08), Europe (0.02) and Oceania (0.03). Predicted population increases show different patterns between urban and rural dryland areas. Populations in urban centers are projected to increase by the end of this century, with a predicted tripling over the African continent. This reflects the profound impact of urbanization on population growth. By contrast, the rural dryland population is expected to shrink over this time period in all regions excluding Africa.

6.1.4 Economic Development in Drylands

Gross domestic product (GDP) is a conventional proxy for economic development. According to global gridded GDP maps (Kummu et al. 2018), dryland countries contributed >25% of the total global GDP over 1990–2015. The average GDP in dryland countries is well below the global average and is distributed unevenly across continents (Fig. 6.5). Asia, Europe, and North America have shown the most rapid GDP growth over the last three decades, with Asia having the most spatially homogeneous growth distribution between dryland and non-dryland areas during 1990–2015.

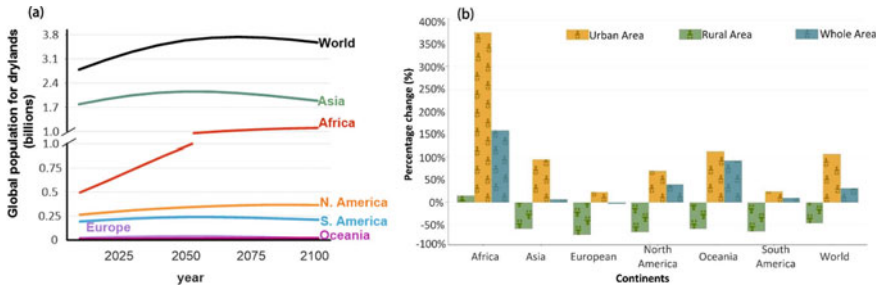


Fig. 6.4 **a** Projected population growth by region from 2010–2100 in current-day dryland areas. **b** Projected changes in population growth by region by 2100, as compared to 2010, for current-day dryland areas. Data were obtained from the Global 1-km Downscaled Population Base Year and Projection Grids provided by the Shared Socioeconomic Pathways database, version 1.01 (2000 – 2100)

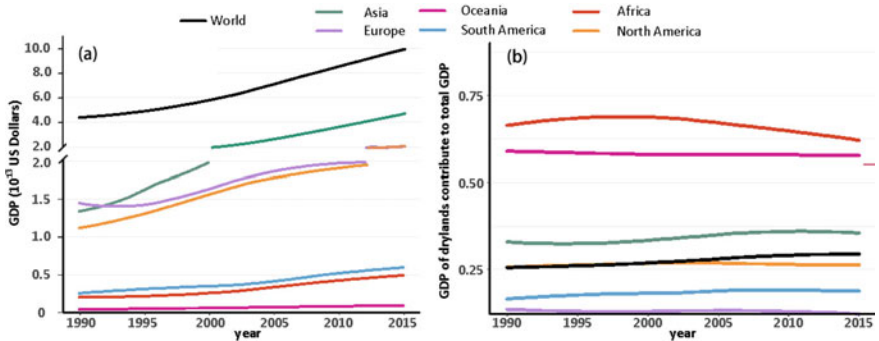


Fig. 6.5 **a** GDP and **b** the contribution of dryland regions to the total GDP for each continent during 1990–2015

In Africa, dryland countries showed less growth than humid ones. Among Asian and African countries, dryland regions typically contribute >50% of the total national GDP (Fig. 6.6). Dryland areas that are highly economically developed are mainly distributed in western Asia, Eastern Europe, East China, and the United States. When overlain with patterns in net migration, it is clear that dryland regions with higher GDP are more strongly associated with net migration gains.

Satellite-derived nighttime light intensity is a robust proxy for human activity (Fig. 6.7). When assessed over decadal time periods, nighttime light intensity illustrates the intensification of human industrial activity, changes in the mosaic of human settlements, and wildfire events. Combined use of population density and nighttime light intensity robustly reflects the relative level of economic development and human wellbeing in specific areas. Although persistent cloud cover can obscure urban centers in some areas like the Amazon and Congo, dryland urban centers tend to have more reliable light measures due to clear nighttime skies. Regions denoted in light grey in Fig. 6.7 represent older established urban centers, whereas those in cyan, yellow,

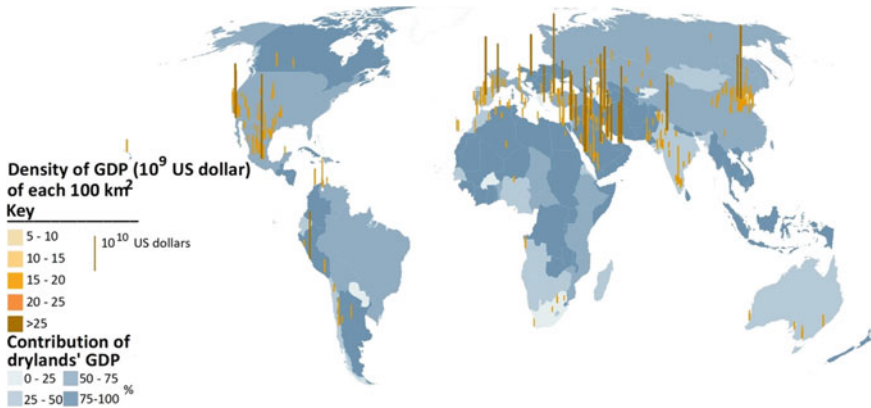


Fig. 6.6 GDP density in global drylands as of 2015. Cells (10×10 km) with a GDP <5 billion are not shown. Bar heights reflect the GDP for each cell. The colors indicate the relative contributions to GDP. Countries that do not have dryland regions are not shown

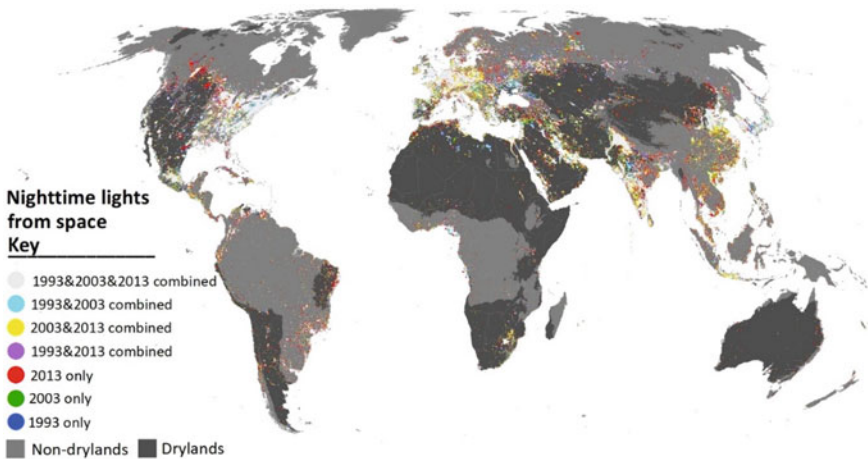


Fig. 6.7 Global patterns of nighttime light intensity (DMSP-OLS) as observed from space. Colors are representative of three annual cloud-free composites: 1993 (blue), 2003 (green), and 2013 (red). The remaining colors indicate changes in nighttime light intensity within this 10-year period

and magenta show urban growth that has occurred during the twenty-first century. Prior to 2003, there were far fewer large urban centers in drylands compared to non-drylands, particularly in Africa, Asia, and South America. More diffuse light over these dryland areas reflects their low levels of infrastructure. Differences in urban growth between dryland and non-dryland areas have been less pronounced in North America.

6.2 Changes in Dryland Ecosystems

6.2.1 Vegetation Greenness

Dryland ecosystems, primarily comprised of savannas, grasslands, and shrublands, are characterized by long-term water stress and high sensitivity to climate fluctuations. Remote sensing techniques provide valuable and continuous data on dryland vegetation at the global scale. However, satellite orbit drift and sensor degradation and replacement have led to uncertainties in the data time series (Jiang et al. 2017; Zhang et al. 2017). We used the most recent versions of multiple remote sensing datasets to systematically assess trends in global dryland vegetation for 1982–2019.

For the assessed period, all remotely sensed vegetation indices indicated significant vegetation growth in arid areas. Leaf area index (LAI) values provided by the Global Inventory Modeling and Mapping Studies (GIMMS) and GLOBMAP both suggested a significant increase in the annual mean LAI in global drylands ($0.013 \text{ m}^2 \text{ m}^{-2} \text{ decade}^{-1}$, $p < 0.01$, and $0.015 \text{ m}^2 \text{ m}^{-2} \text{ decade}^{-1}$, $p < 0.01$, respectively; Fig. 6.8). This trend was further supported by the GIMMS normalized difference vegetation index (NDVI) 3 g, which indicated a significant increase in the greenness of global dryland vegetation ($0.003 \text{ decade}^{-1}$, $p < 0.01$; Fig. 6.8). Although several studies reported a slowdown of the greening of dryland vegetation after 2000 (Gonsamo et al. 2021; Yuan et al. 2019), recent Moderate Resolution Imaging Spectroradiometer (MODIS) vegetation indices consistently suggest that this trend is continuing and evolving (Fig. 6.8). Notably, MODIS LAI suggests a larger increase in LAI over the period 2003–2019 ($0.036 \text{ m}^2 \text{ m}^{-2} \text{ decade}^{-1}$, $p < 0.01$; Fig. 6.8) than the LAI estimates provided by GLOBMAP and GIMMS.

Greening trends are not uniform across drylands, as shown in the spatial pattern of annual mean LAI in dryland vegetation over the past three decades (Fig. 6.9). The two long-term LAI datasets showed consistent greening and browning trends (Fig. 6.9), mainly in North/Central America, western India, Inner Mongolia, southern Sahara, South Africa, and eastern Australia. By contrast, browning trends were clearly shown in west Asia, central and southern South America, and northwestern Australia. Globally, greening trends increase along with the aridity index (Fig. 6.9). Based on GIMMS LAI3g data, the changes in annual mean LAI across hyper-arid (aridity index < 0.05), arid ($0.05 \leq$ aridity index < 0.2), semiarid ($0.2 \leq$ aridity index < 0.5), and sub-humid arid ($0.5 \leq$ aridity index < 0.65) regions are $0.004 \text{ m}^2 \text{ m}^{-2} \text{ decade}^{-1}$, $0.005 \text{ m}^2 \text{ m}^{-2} \text{ decade}^{-1}$, $0.014 \text{ m}^2 \text{ m}^{-2} \text{ decade}^{-1}$, and $0.024 \text{ m}^2 \text{ m}^{-2} \text{ decade}^{-1}$, respectively. These trends were also consistent with GLOBMAP estimates (Fig. 6.9).

Driving mechanisms of dryland vegetation changes

Dryland greening, as observed by satellites, is an integrated response vegetation to environmental change. Understanding and quantifying the contribution of individual environmental factors to dryland vegetation growth is challenging yet critical research highlights (Lian et al. 2021; Piao et al. 2020; Zhu et al. 2016). Among many

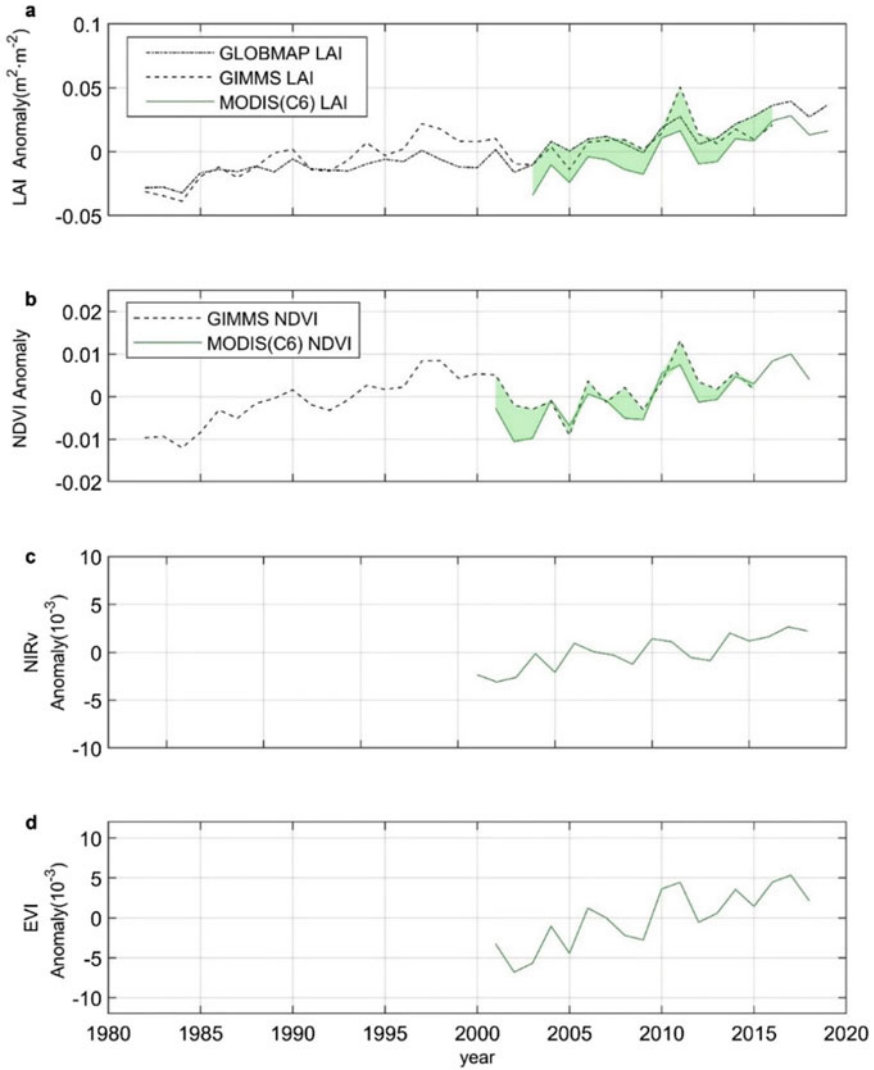


Fig. 6.8 Changes in satellite-derived vegetation indices and solar-induced fluorescence in global drylands. **a** Leaf area index (LAI) from three products: GIMMS LAI3g (Zhu et al. 2013), GLOBMAP LAI (Liu et al. 2012), and MODIS LAI (Myneni et al. 2002; Yan et al. 2016). **b** Normalized difference vegetation index (NDVI) from GIMMS NDVI3g (Pinzon and Tucker 2014) and MODIS C6 (Huete et al. 2002). **c** Near-infrared reflectance of terrestrial vegetation (NIRv) (Badgley et al. 2017). **d** Enhanced vegetation index (EVI) from MODIS C6 (Huete et al. 2002)

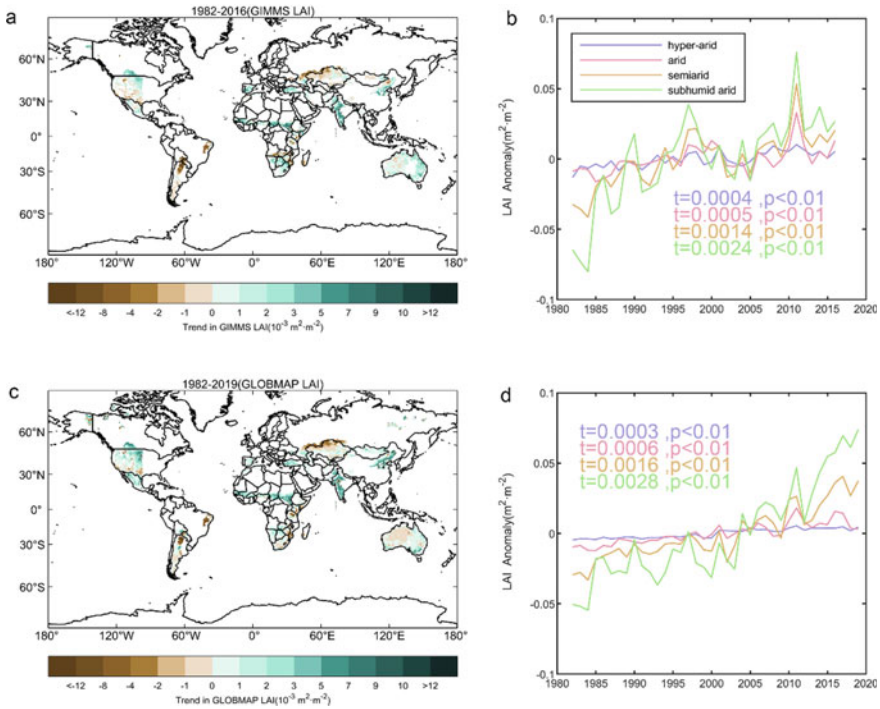


Fig. 6.9 Spatial pattern of changes in annual mean leaf area index (LAI) in global drylands during 1982–2019 from **a** GIMMS LAI3g (Zhu et al. 2013) (1982–2016), **b** GIMMS LAI3g over four dryland categories (hyper-arid, arid, semiarid, sub-humid arid), **c** GLOBMAP LAI (Liu et al. 2012), and **d** GLOBMAP LAI over four dryland categories

environmental changes, increasing atmospheric CO₂ concentration, climate change, nitrogen deposition, and land cover change have been widely assessed and identified as the major driving factors of dryland greening (Piao et al. 2020; Zhu et al. 2016).

We used an ensemble of eight state-of-the-art ecosystem models (CLM5, ISAM, ISBA-CTRIP, JULES-ES-1.0, LPJ-GUESS, ORCHIDEEv3, DLEM, and ORCHIDEE) to quantify the contributions of elevated atmospheric CO₂ concentration, climate change, and land cover change to the satellite-observed trends in the annual mean LAI of global dryland vegetation during 1982–2016 (Fig. 6.10). Factorial simulations included no forcing change (S0); varying CO₂ only (S1); varying CO₂ and climate (S2); and varying CO₂, climate, and land use (S3). Simulation S3 forced by all environmental factors well captured the interannual variation in annual mean LAI (Fig. 6.10). The correlation coefficients between the model-simulated LAI, GIMMS LAI, and GLOBMAP LAI time series were 0.83 ($p < 0.01$) and 0.85 ($p < 0.01$), respectively. GIMMS LAI3g and GLOBMAP LAI both suggested a significant increase in annual mean LAI ($0.013_{0.012}^{0.014, GLOBMAP}$ m²m⁻² decade⁻¹, $p < 0.01$) during 1982–2016. Ecosystem models to some extent reproduced the observed greening trends but with notable uncertainties ($0.018_{-0.001, ISAM}^{0.030, JULES-ES-1.0}$ m²m⁻²

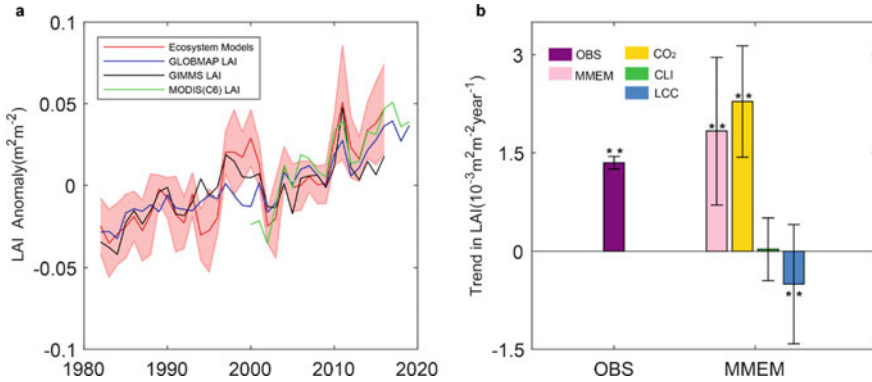


Fig. 6.10 Changes in the annual mean LAI of global dryland vegetation and its driving factors. **a** GIMMS LAI3g, GLOBMAP LAI, and MODIS LAI. **b** The relative contribution of increasing atmospheric CO₂ concentration (CO₂), climate change (CLI), and land use and land cover change (LCC) to the LAI trends simulated by the ensemble ecosystem models

decade⁻¹, $p < 0.01$). Overall, consistency between the modeled simulations and remotely sensed data provides confidence for using ecosystem models in attribution analyses.

Factorial simulations of ecosystem models provide an effective means to quantify the major drivers of global dryland vegetation change (Piao et al. 2020; Zhu et al. 2016). The contributions of atmospheric CO₂ concentration, climate change, and land cover change to changes in LAI were quantified using S1–S0, S2–1, and S3–S1, respectively.

Rising atmospheric CO₂ concentration. The fertilization effect of elevated atmospheric CO₂ has been quantified in open-top-chamber experiments (Drake et al. 1989; Leadley and Drake 1993) and free-air CO₂ enrichment (FACE) experiments (Norby et al. 2010; Norby and Zak 2011). Increased atmospheric CO₂ contributed $0.023_{-0.001, ISBA-CTRIIP}^{0.033, CLM5.0}$ m²m⁻² decade⁻¹ ($p < 0.01$) to the global LAI (Fig. 6.10). Relative to other vegetation types, CO₂ fertilization effects are more prominent in drylands, where elevated CO₂ concentration alleviates water stress by reducing stomatal apertures and increasing the water use efficiency (WUE) of plants (Donohue et al. 2013; Lian et al. 2021). The simulations suggested that the effects of CO₂ fertilization on global vegetation growth have been uniformly positive over the past three decades (Fig. 6.11). However, this trend may decline as other environmental factors start to limit plant physiology (Hovenden et al. 2019; Norby et al. 2010; Reich et al. 2014; Terrer et al. 2016).

Climate change. Climate change contributed $0.0003_{-0.007, CLM5.0}^{0.008, ORCHIDEE}$ m²m⁻² decade⁻¹ ($p = 0.92$) to the global dryland LAI (Fig. 6.10). In contrast to the uniform effect of CO₂ fertilization, the effect of climate change on global dryland vegetation is notably heterogeneous (Fig. 6.11). Positive effects dominated vegetation growth in >55% of the vegetated land in the northern and southern high latitudes (north of 50°N

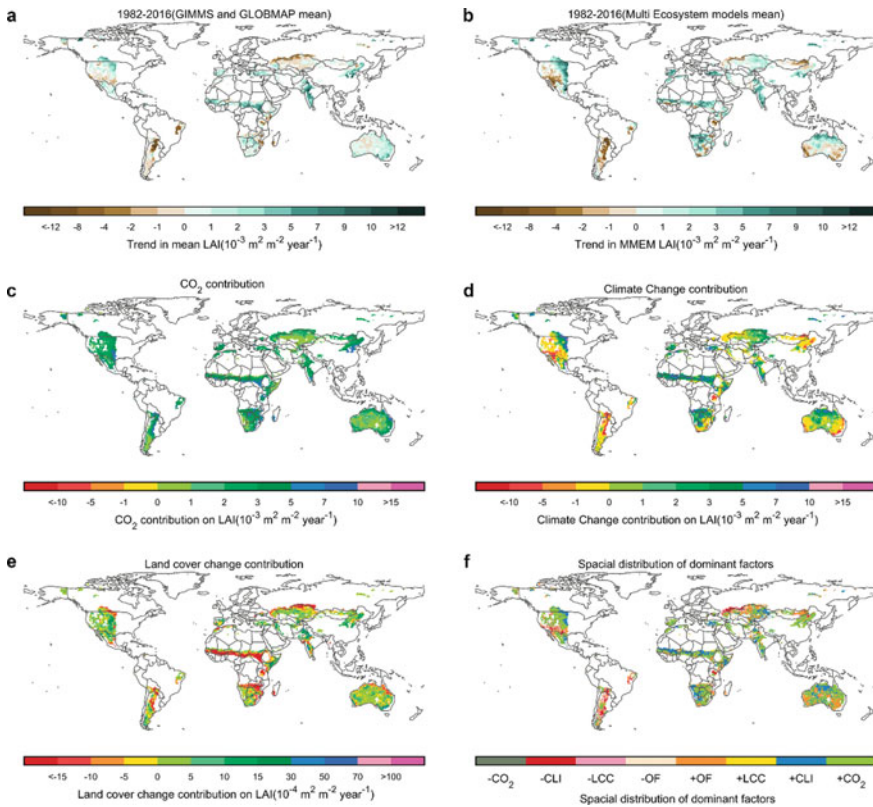


Fig. 6.11 Attribution analysis of trends in the annual mean LAI across global drylands. **a** Satellite-observed LAI trends. **b** Model-simulated LAI trends. **c** CO₂ fertilization effects. **d** Effects of land cover change. **e** Effects of climate change. **f** The dominant factors that drive annual mean LAI. Other factors (OF) are defined as the fraction of the observed LAI trends not accounted for by modeled factors. The prefix ‘+’ indicates a positive effect of the corresponding driver on LAI trends, and the prefix ‘-’ indicates a negative effect

and south of 50°S, respectively) and the Tibetan Plateau. This is due to increased air temperature extending the growing season and enhancing photosynthesis in these regions (Keenan and Riley 2018; Xu et al. 2013). Global-scale precipitation redistribution, including the amount, seasonality, and frequency, is also likely to be an essential driver of the heterogeneity of climate change effects (Ukkola et al. 2021; Zhu et al. 2017). Overall, there were low net effects due to climate change, caused by positive effects offsetting negative ones.

Land cover change. As human societies have highly developed, natural vegetation has been cleared for agriculture, but large swaths of croplands have since been abandoned, and natural vegetation has regrown in these areas (Foley et al. 2005; Song et al. 2018). Current ecosystem models partially represent these biogeographical processes, which strongly affect regional vegetation greenness

(Hansen et al. 2013; Piao et al. 2018; Zhu et al. 2016). The ensemble ecosystem models suggested that land cover change contributed $-0.005_{-0.018, LPJ-GUESS}^{0.005, ORCHIDEEv3}$ $\text{m}^2\text{m}^{-2} \text{decade}^{-1}$ ($p < 0.01$) to the global LAI. Positive effects of land cover change were most prominent in regions with extensive agricultural activity, whereas areas affected by negative change tended to be clustered in western Asia, southern Sahara, and South Africa. Notably, the conversion of agricultural land to forest (reforestation) and large plantation forest programs (afforestation) have also greatly contributed to the greening of vegetation in these regions (Chen et al. 2019; Song et al. 2018).

Other factors. The unexplained portion of the satellite-derived LAI trends was determined by subtracting the satellite-derived trends from the trends simulated by the TRENDY models considering all driving factors (Fig. 6.11). We consider this unexplained variation to have been driven by other factors (OF). OF effects are likely best summarized into three categories: uncertainties in satellite observations, misrepresentation of processes in the ecosystem models, and missed processes in the ecosystem models. Interestingly, OF effects are not widely represented in Fig. 6.11. This indicates that current ecosystem models can reasonably reproduce satellite-derived LAI trends. Nevertheless, ecosystem models still require improvement in terms of their ability to represent processes associated with agricultural activities, forest aging, other regionally important ecosystems such as wetlands and peatlands, and disturbances (Chazdon et al. 2016; Kantzas et al. 2015; Pan et al. 2011; Zhou et al. 2015).

6.2.2 Land Cover Change

Drylands occupy approximately 42% of the total land area globally, with predominant types including grasslands, shrublands, croplands, and barren lands (Fig. 6.12). In a MODIS-derived land cover product, grasslands comprise 40.5% of global drylands, followed by barren lands (33.2%), shrublands (15.5%), and croplands (10.1%). These natural and semi-natural lands provide invaluable ecosystem services for human populations. Globally, grasslands are mainly distributed in western America, western Asia, northern Mongolia, Inner Mongolia, southern Sahara, eastern and southern Africa, and northern and eastern Australia. Croplands in drylands are concentrated in the Northern hemisphere, i.e., northwestern America and western India. Shrublands are concentrated in the Southern hemisphere, including central Australia, southern Arica, and southern South America.

Dryland land cover types are vulnerable to environmental change and anthropogenic activity, and dryland land cover has changed significantly due to these factors (Song et al. 2018). We quantified land cover change in drylands during 2001–2019 using an annual MODIS-derived land cover product (Fig. 6.13). The most significant change over this period was the interconversion of grassland and shrubland. Approximately $9.7 \times 10^5 \text{ km}^2$ of grassland was converted to shrubland, and $9.3 \times 10^5 \text{ km}^2$ of shrubland was converted to grassland during this period. Approximately $2.7 \times$

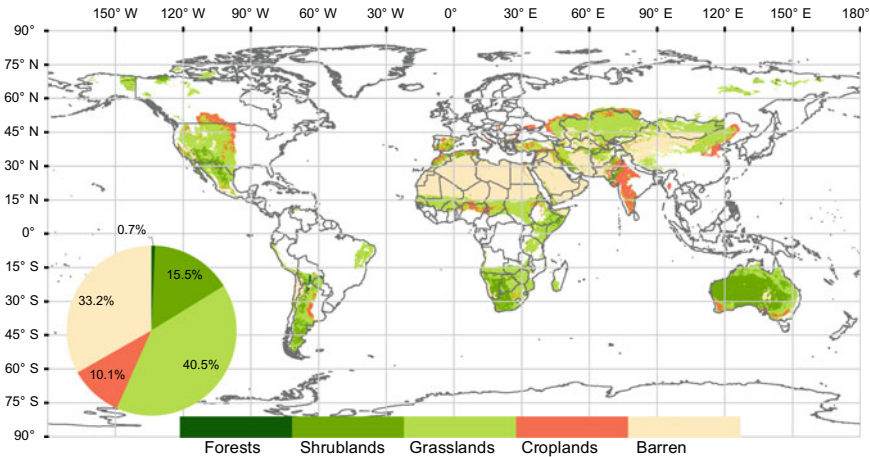


Fig. 6.12 Global pattern and proportion of land cover in drylands during 2019. The pie chart represents the proportion of each land cover type. The most common land cover types in arid areas are grasslands and barren lands, followed by shrublands and croplands

10^5 km² of vegetation dryland was converted to barren land, but 7.2×10^5 km² of barren land was converted to a vegetated land cover type, primarily grassland (4.2×10^5 km²) and shrubland (2.9×10^5 km²). Overall, global drylands now have more vegetated land cover than they were in 2000.

Spatial patterns of land cover change are strongly heterogeneous (Fig. 6.14). Conversion from other land cover types to cropland was concentrated in the northern hemisphere, mostly in northeastern America, western India, and Inner Mongolia. Transitions among natural vegetation types was more prevalent in drylands south of 15°S. A notable fraction of barren lands has been converted to grasslands in northwestern China. The same land cover transition was also observed in the southern belt of the Sahara. It appears that environmental changes, including increased CO₂ concentration and altered precipitation, are promoting vegetation encroachment in these regions (Li et al. 2018; Lian et al. 2021; Ukkola et al. 2021).

Land cover change in drylands at the global scale influences profoundly climate feedback systems and human societies (Lian et al. 2021). In the context of global environmental changes, quantifying land cover change in arid areas and elucidating the driving mechanisms are vital for both current understanding and future predictions of ecosystem services (Zelnik et al. 2013). Future efforts to formulate land management strategies and policies in arid areas could benefit from quantifying the interactions between natural environmental change and human activities under climate change (Burrell et al. 2020; Tian et al. 2019).

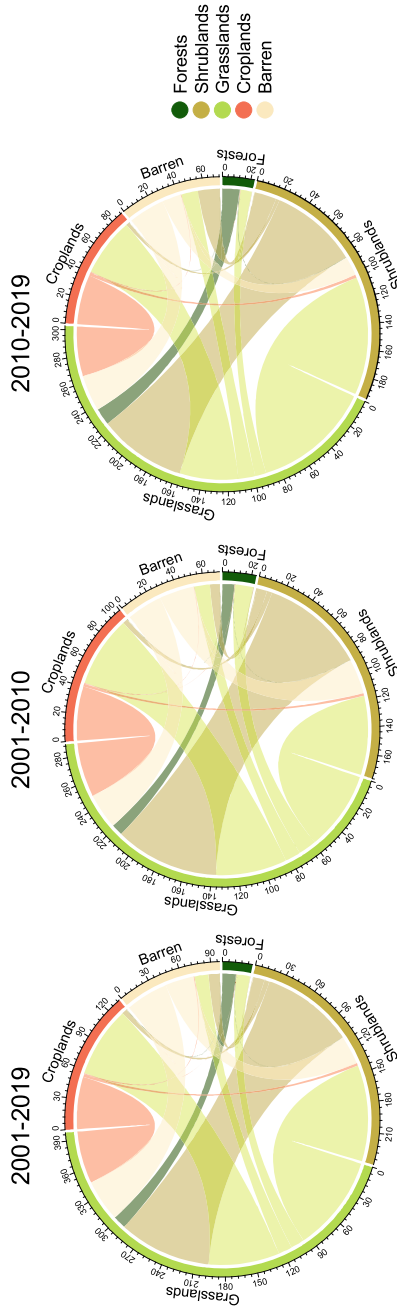


Fig. 6.13 Land cover changes over three periods; 2001–2019, 2001–2010, and 2010–2019. Numbers indicate the amount of converted lands (10^4 km^2). Colors indicate the total change in land cover type. The change in land cover type is represented by the position of the chord and ring; identical colors represent a loss of that type, and different colors represent a gain

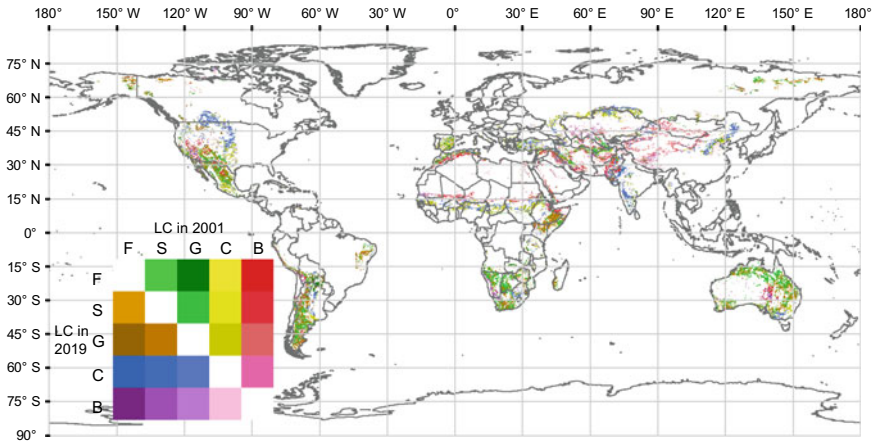


Fig. 6.14 Global pattern of land cover change during 2001–2019. F, S, G, C, and B indicate forests, shrublands, grasslands, croplands, and barren land, respectively

6.3 Changes in Ecosystem Functions in Drylands

6.3.1 Ecosystem Productivity

Gross primary productivity (GPP) is the amount of carbon fixed by vegetation through photosynthesis, which is a critical component of the terrestrial carbon cycle. Quantification of GPP from regional to global scales is important for understanding the feedbacks of terrestrial ecosystem to climate change (Le Quéré et al. 2009; Piao et al. 2009; Sitch et al. 2015). In drylands where long-term and continuous field observations are scarce, remote sensing is a primary approach for monitoring vegetation functional dynamics at broad scales (Smith et al. 2019). Another alternative to observations is dynamic global vegetation models (DGVMs) which simulate major biochemical processes in terrestrial ecosystems. Such models have been widely used to study spatiotemporal variability in global and regional carbon cycles and its driving processes.

We used DGVMs to estimate annual mean GPP in drylands during 1980–2019. An annual average GPP is about $29 \pm 5.0 \text{ Pg C yr}^{-1}$, with larger values distributed in transition zones between dry and wet regions (Fig. 6.15). Dryland ecosystems in Australia, USA, and Brazil had the highest annual mean GPP values, which together comprised 27% of the global total GPP. Dryland ecosystems comprise 91% of the total land area in Australia. Consistently, satellite-observed solar-induced fluorescence (SIF), as a robust proxy for GPP, also showed a similar spatial pattern (Fig. 6.15) of enhanced productivity.

According to the DGVMs, dryland GPP increased significantly at an average rate of $0.10 \text{ Pg C yr}^{-2}$ during 1980–2018 (Fig. 6.16), partly contributing to the overall growth in global GPP over the same period (Campbell et al. 2017). SIF showed

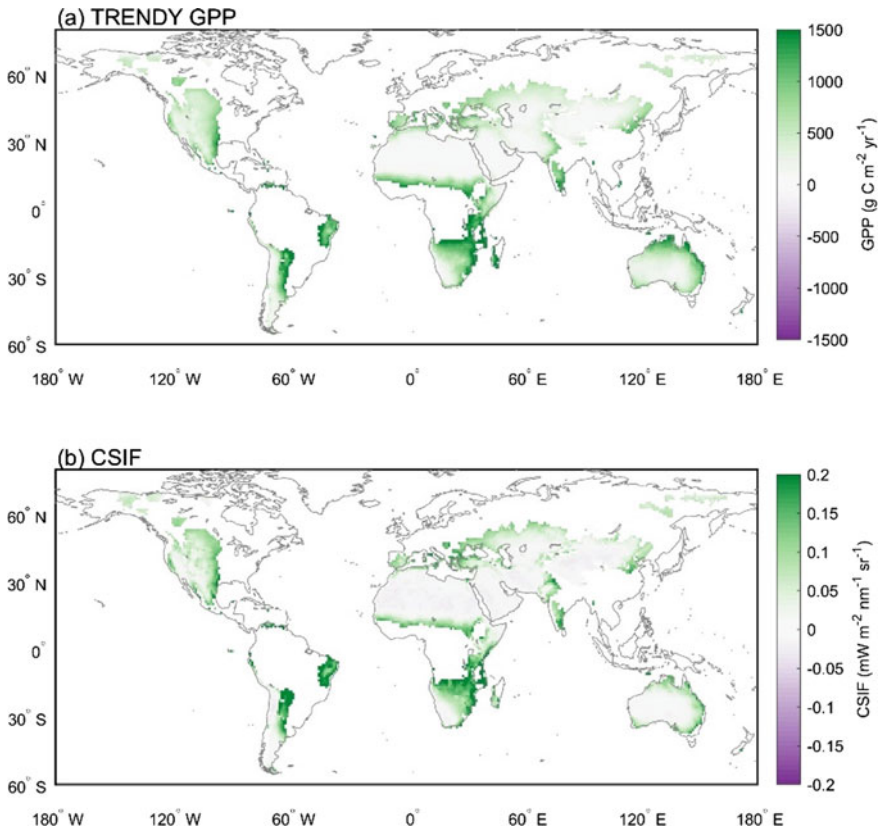


Fig. 6.15 Spatial distributions of gross primary productivity (GPP) and solar-induced fluorescence (SIF) across drylands during 1980–2018. **a** Spatial patterns of annual mean GPP estimated from multiple dynamic global vegetation models (DGVMs) provided by the TRENDY project. **b** Spatial patterns of annual mean SIF, obtained from a contiguous solar-induced chlorophyll fluorescence (CSIF) product (Zhang et al. 2018), during 2000–2018

similar interannual variations, with a significantly increasing trend in dryland ecosystems during 1980–2018 (Fig. 6.16). Increased CO_2 concentration, climate change, and land cover change are likely to drive this pattern. Increased atmospheric CO_2 directly stimulates photosynthesis, and indirectly by reducing stomatal conductance and elevating water use efficiency (Lian et al. 2021; Piao et al. 2020). Factorial simulations from multiple DGVMs suggest that CO_2 fertilization accounted for $91 \pm 20\%$ of the GPP trend in 1980–2018 (Fig. 6.16). The fertilization effect of CO_2 is particularly prevalent in drylands, where positive enhancement of GPP was seen over 94% of drylands (Fig. 6.17). This effect was greatest in Australia, followed by the United States and China, countries with the greatest area of drylands globally.

In contrast to the straightforward positive influence of CO_2 fertilization, climate change contributed both positively and negatively to dryland GPP trends from 1980 to

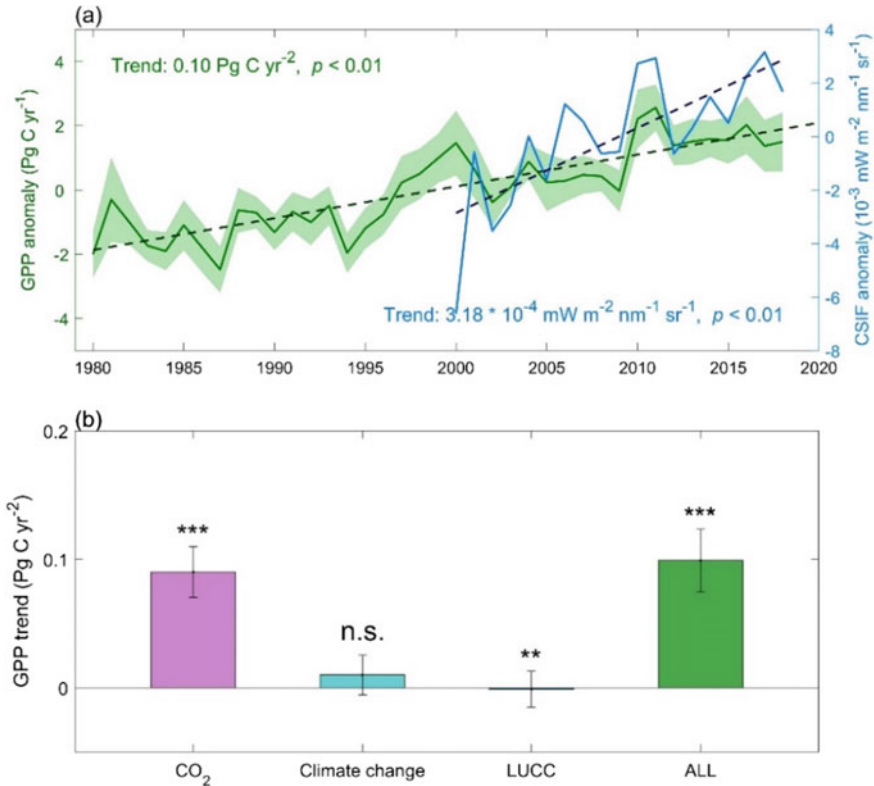


Fig. 6.16 Trends in GPP and SIF, and attribution analysis of GPP trends in drylands. **a** Temporal variation in annual mean GPP from multiple DGVMs provided by the TRENDY project (1980–2018), and the annual mean SIF obtained from a CSIF product (2000–2018). **b** Attribution analysis of the DGVM-estimated GPP trend (1980–2018): effects of CO₂ fertilization, climate change, and land cover and use change, and the overall GPP trend. Error bars represent standard deviations across multiple DGVMs. Stars represent significance levels for the estimated GPP trend. ****p* < 0.01; ***p* < 0.05; **p* < 0.1; n.s., *p* > 0.1

2018 (Fig. 6.17). Climate change had a significant effect for 32% of the total dryland area globally, with larger positive effects on the GPP trend seen in the United States, Canada, and Sudan, and larger negative effects observed in Australia and Brazil. Climate change explained approximately 10 ± 16% of the total GPP trend, but this influence was not significant across global dryland ecosystems due to the balance of positive and negative effects (Fig. 6.16). Despite large model spread, land cover and use changes had a significant, albeit small, negative effect (−1.1 ± 14%), on the GPP trend (Fig. 6.16). Spatially, positive effects of land cover and use changes were found in Sudan, India, and China, whereas strong negative effects were found in Russia, Australia, and the United States (Fig. 6.17). The expansion of forest and cropland cover in China and India (Chen et al. 2019) has positively influenced GPP.

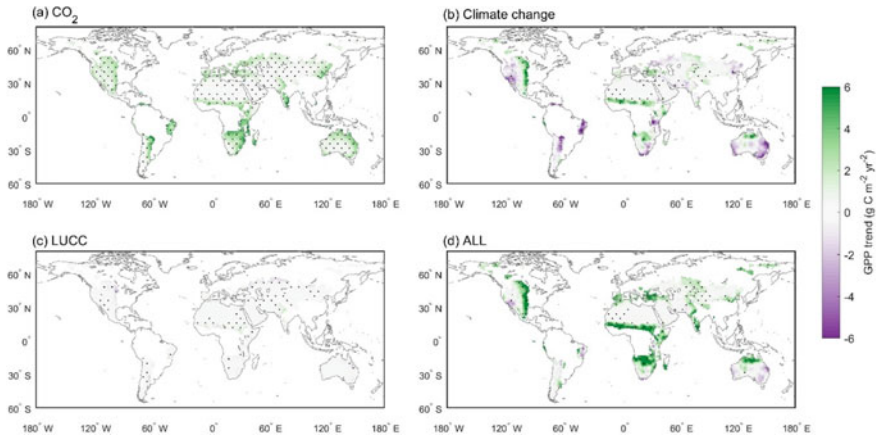


Fig. 6.17 Spatial patterns obtained by attribution analysis of dryland GPP trends during 1980–2018. **a** CO₂-induced dryland GPP trend estimated from multiple DVGMs. **b** Climate change-induced dryland GPP trend calculated from ensemble DGVMs. **c** Land cover and use change-induced dryland GPP trend estimated from multiple DGVMs. **d** Dryland GPP trend simulated from multiple DGVMs. Stippling indicates pixels with a significant GPP trend ($p < 0.05$)

Overall, the CO₂ fertilization effect was the main driver of the increasing trend in GPP in 63% of the dryland countries globally, including Australia, the United States, and China. Climate change was the main driver for 37% of dryland countries, including Sudan. Among all countries, the increasing trend in GPP was strongest in dryland areas of the United States ($8.32 \pm 3.83 \times 10^{-3}$ Pg C yr⁻²), Sudan ($5.81 \pm 3.92 \times 10^{-3}$ Pg C yr⁻²), and China ($5.31 \pm 4.58 \times 10^{-3}$ Pg C yr⁻²). Significant increases in dryland GPP were clustered in the central United States, Sahel, southern Africa, India, and northern Australia. Small decreases in GPP in drylands were found in the southwestern United States, eastern Brazil, and eastern Australia (Fig. 6.17).

Whether the beneficial effect of CO₂ fertilization on photosynthesis vegetation will persist into a warmer and drier future is of critical concern. Simulations under RCP8.5, obtained from multiple earth system models (ESMs) provided by the Coupled Model Intercomparison Project Phase 5 (CMIP5), predict a linear enhancement of GPP in drylands over the twenty-first century (Fig. 6.18), in response to higher CO₂ and associated climate change. Large increases in GPP are predicted for drylands in southern South America, Sahel, southern Africa, India, and northern China (more than $600 \text{ g C m}^{-2} \text{ yr}^{-1}$ by the end of the century). GPP increases in dryland contribute substantially to global GPP increases, which could help slow down the warming and increase ecosystem service provisioning. However, there is substantial variation in GPP estimates derived from different DGVMs and ESMs, due to differences in how vegetation structure and function are simulated (Anav et al. 2013; Murray-Tortarolo et al. 2013; Wang et al. 2011). Therefore, greater efforts to improve model structures and benchmark model results are still needed. Expanding field observations in drylands, combining data from multiple sources, and developing

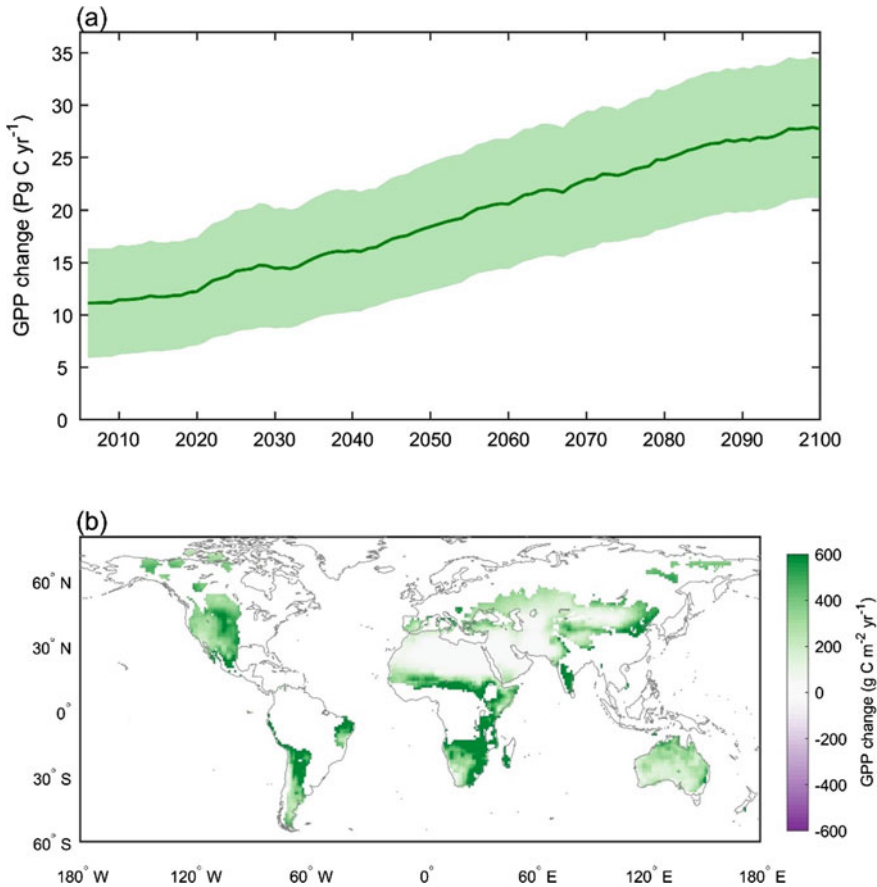


Fig. 6.18 Changes in annual mean GPP under RCP 8.5. **a** Temporal variation in GPP change during 2006–2100 estimated from multiple earth system models (ESMs) in CMIP5. Data have been smoothed with a 5-year running window. Shaded areas represent the standard error among different ESMs. **b** GPP change predicted using multiple ESMs in CMIP5 for 2081–2100 relative to 1986–2005

suitable algorithms for dryland ecosystems are especially important for monitoring and predicting variation in GPP in these areas (Smith et al. 2019).

Croplands are nonnegligible parts of the global dryland ecosystems, which provide the major food sources in humans' daily life. In contrast to the GPP used for the natural vegetation growth, crop yield is a more representative index of the productivity of the agricultural ecosystems. Wheat, rice, maize, and soybeans are the world's 'four' staple foods, which provide two-thirds of human caloric intake (Tilman et al. 2011). Thus, yield changes for these four major crops were assessed in the global dryland ecosystems.

The historical yield data used here were from a recently released global gridded dataset of historical yields for major crops (GDHY), which is a hybrid of agricultural census statistics from FAOSTAT and satellite remote sensing (Iizumi and Sakai 2020). According to the GDHY dataset, the crop yields in the dryland increased significantly at an average rate of $0.019\text{--}0.051\text{ t ha}^{-1}\text{ yr}^{-1}$ during 1982–2016 (Fig. 6.19), that is to say an increase of 200–300% during the past 35 years. The average yield of maize (C4 crop) was higher than wheat, rice and soybean (C3 crop), but the relative change was smaller than the other three crops. Factorial simulations from global gridded crop model (GGCM; EPIC, GEPIC, pDSSAT, LPJ-GUESS, LPJmL, and PEGASUS) intercomparison, coordinated by the Agricultural Model Intercomparison and Improvement Project (AgMIP) (Rosenzweig et al. 2013) as part of the Inter-Sectoral Impact Model Intercomparison Project (ISI-MIP) (Warszawski et al. 2014) indicate that yield changed little due to the climate change from 1980 to 2005 (Trend = $-0.001\text{--}0.002\text{ t ha}^{-1}\text{ yr}^{-1}$). Therefore, the historical reported yield increase of 200–300% in the drylands might be attributed mainly to the technology advances and management improvements, such as modern cultivars applications, more harvesters, fertilizers and irrigation inputs, and advanced pest and diseases controls.

The spatial patterns of yield trends (Fig. 6.20) also indicate that most of crop-lands in the drylands experienced the obvious yield increases, except some specific crops in hot regions (e.g., wheat and maize in East Africa, and wheat in North Australia). The north part of dryland regions, such as North America, Europe, and North China (yield trends were all above $0.05\text{ t ha}^{-1}\text{ yr}^{-1}$), dominate the boosting of global crop yield during the last three decades. The GGCMs simulated yield trends due to climate change were much smaller than the statistical trends across most of

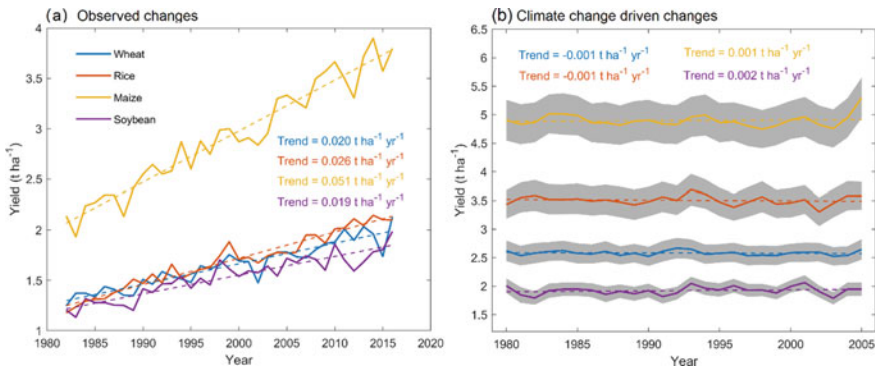


Fig. 6.19 Historical trends of crop yields from observations and climate change driven simulations in the drylands. **a** Temporal variation in annual mean yield of major crops provided by the GDHY (1982–2016), a reanalysis dataset based on the FAOSTAT database. **b** Global gridded crop models (GGCMs) simulated yield trend (1980–2005) from the climate change impact. The absolute yields from simulations were higher than those from the census statistics, due to the potential management conditions by simulations. The grey shades represent the standard errors from the ensembles of thirty members (five crop models coupled with five global climate models)

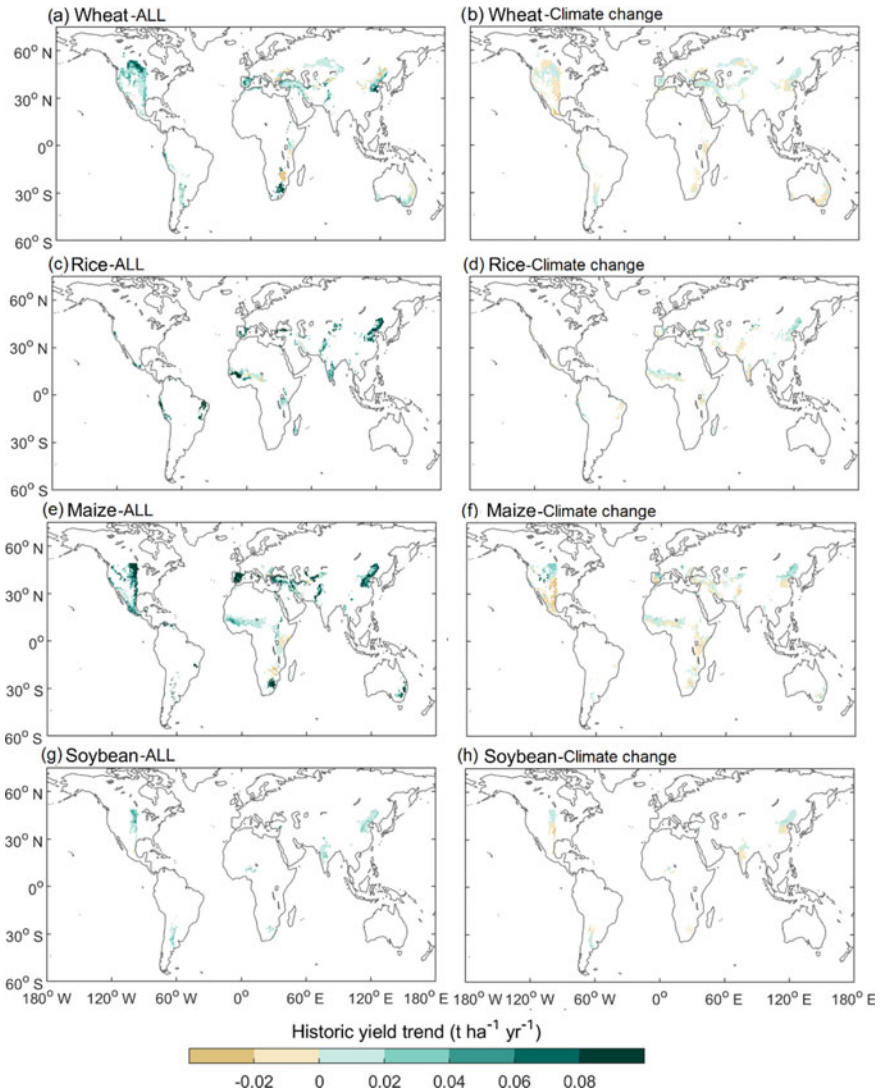


Fig. 6.20 Spatial patterns of crop yield trends in the drylands obtained from GDHY observations (1982–2016) and GCMs simulations driven by climate change (1980 – 2005). **a, c, e, g** Observed yield trend for wheat, rice, maize and soybeans. **b, d, f, h** Simulated yield trend driven by climate change for wheat, rice, maize, and soybeans

regions. However, the historical climate change impact on yield shows considerable heterogeneity across the studied regions. The north parts of drylands benefited from the climate change, but the south parts suffered the yield loss. The contrast between impacts on the north and south of drylands might be related to the differences in the

background climate, especially the temperature (Challinor et al. 2014; Zhao et al. 2016).

The future yield changes were assessed with the GCMs ensembles coupled with 5 global climate models (GCMs). The patterns of ensemble medians (Fig. 6.21) show that under RCP 2.6 scenario, if the CO₂ effects were not considered, the crop yield changes until the end of century (2070–2099) will be positive or negative across regions, similar to the patterns of historic trend but with a larger magnitude. In general, wheat, rice, and soybeans in the north part of America, Europe, and Asia will generally have yield gains, up to 10% relative to the baseline period; Africa and some hot regions might have slight negative yield changes. For maize, large parts of the drylands might suffer yield loss, especially in Africa (up to 50% of yield loss) where hungers already happened. If the climate becomes warmer, from RCP 2.6 to RCP 4.5 scenario, more regions will see the yield loss and the regions with negative impact might become more vulnerable. Overall, to the end of this century, the climate scenario of RCP 2.6 (RCP 4.5) will change the average yield of wheat, rice, maize, and soybeans for the global drylands by 1.2% (−5.7%), −2.1% (−7.2%), −12.3% (−14.1%), and −9.2% (−17.9%), respectively.

6.3.2 Carbon Sink

Despite relatively low mean productivity, vegetation in drylands dominates trends and interannual variability in the terrestrial carbon sink (Ahlström et al. 2015; Poulter et al. 2014). Dryland ecosystems acted as carbon sinks during 1980–2018, as indicated by the annual mean net biome production (NBP) of $0.25 \pm 0.19 \text{ Pg C yr}^{-1}$ (Fig. 6.22a) estimated by an ensemble of 14 DGVMs from the TRENDY project. Three countries fixed more carbon than any others during this time period, including the United States ($0.038 \pm 0.019 \text{ Pg C yr}^{-1}$), Australia ($0.030 \pm 0.033 \text{ Pg C yr}^{-1}$), and Russia ($0.022 \pm 0.015 \text{ Pg C yr}^{-1}$). However, there was a large interannual variation in NBP during 1980–2018, resulting in a non-significant increasing trend of $0.0064 \pm 0.0093 \text{ Pg C yr}^{-2}$.

Increasing atmospheric CO₂ concentration, climate change, and land cover and use changes are the three main drivers of variation in global carbon sinks (Le Quéré et al. 2009; Piao et al. 2009; Sitch et al. 2015). According to DGVM factorial simulations, the CO₂ fertilization effect ($0.0084 \pm 0.0036 \text{ Pg C yr}^{-2}$; $p < 0.01$) dominated the increase in dryland GPP (Fig. 6.16b), thus significantly contributing to the NBP trend (Fig. 6.22b). However, large increases in NBP were offset by significant reductions ($-0.0049 \pm 0.0039 \text{ Pg C yr}^{-2}$; $p < 0.01$) caused by land cover and use changes, which was a carbon source during 1980–2018. Although drylands are sensitive to climate, climate change explained a non-significant proportion of the total NBP ($0.0029 \pm 0.0077 \text{ Pg C yr}^{-2}$; $p > 0.1$). Overall, the trend in NBP of dryland ecosystems was not significant during 1980–2018, and the DGVMs showed marked cross-model variations in dryland carbon sinks (Fig. 6.22).

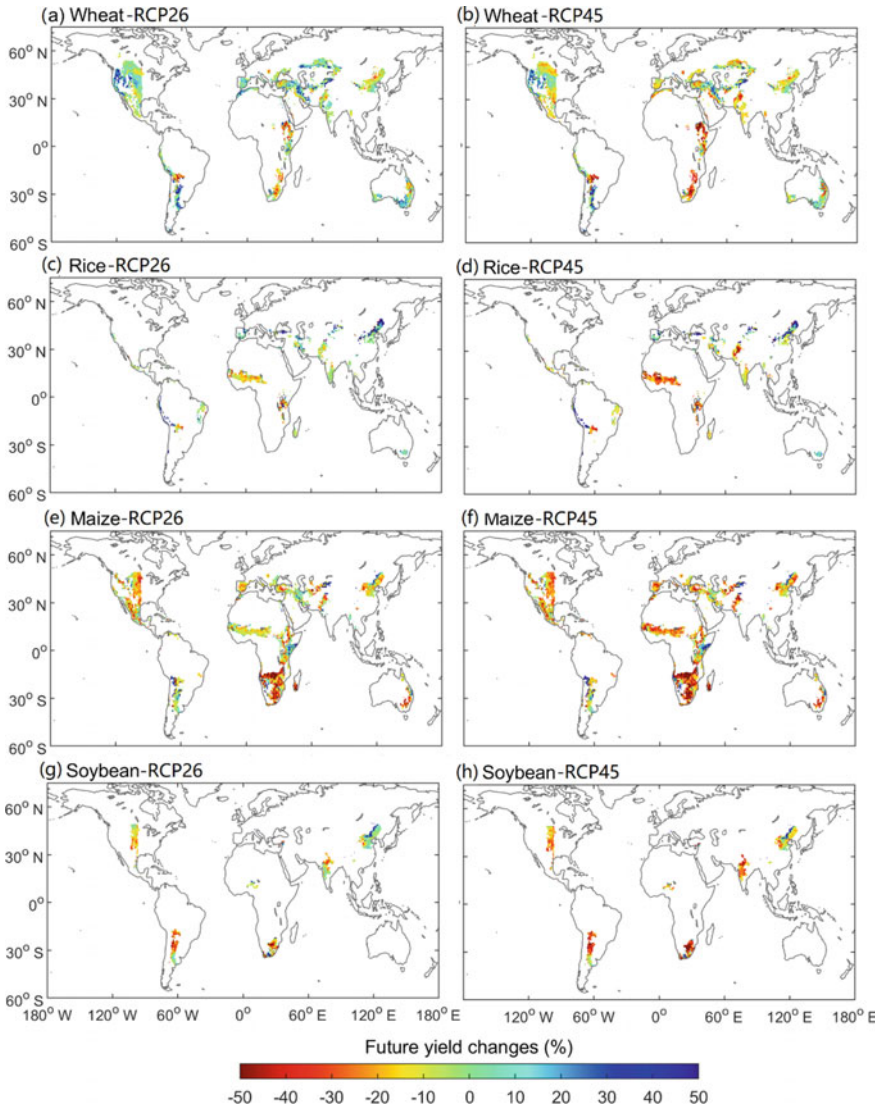


Fig. 6.21 Median crop yield changes (%) for RCP 2.6 and RCP 4.5 (2070 – 2099 in comparison to 1971 – 2005) without CO₂ effects over all five GCMs × six GGCMs simulations in the drylands. **a, c, e, g** Simulated yield changes for RCP2.6 for wheat, rice, maize, and soybean. **b, d, f, h** Simulated yield changes for RCP4.5 for wheat, rice, maize, and soybeans

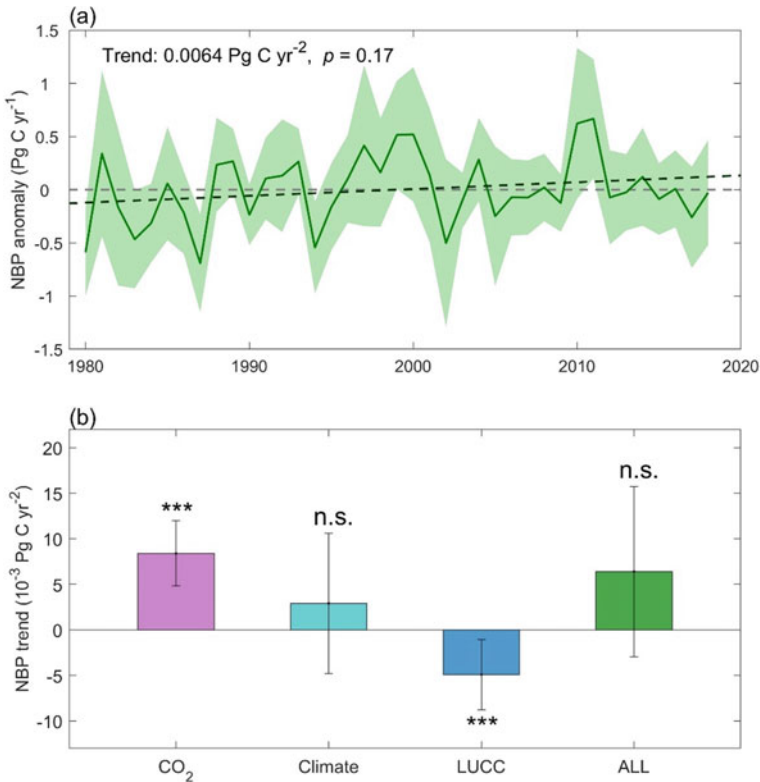


Fig. 6.22 Trends in net biome production (NBP) in drylands and attribution analysis of the NBP trend for 1980–2018. **a** Temporal variation in annual mean NBP from multiple DGVMs obtained from the TRENDY project, and the annual mean SIF from a CSIF product (2000–2018). **b** Attribution analysis of the DGVM-estimated NBP trend: effects of CO₂ fertilization, climate change, and land cover and use change, and the overall NBP trend. Error bars represent standard deviations across multiple DGVMs. Stars represent significance levels for the estimated NBP trend. *** $p < 0.01$; ** $p < 0.05$; * $p < 0.1$; n.s., $p > 0.1$

The CO₂ fertilization effect enhanced NBP over almost all dryland regions in 1980–2018 (Fig. 6.23). Similar to the role of CO₂ fertilization in GPP trends (Fig. 6.17), greater increases in NBP were found in transitional areas between dry and wet regions. There was a large spatial variation in the effect of climate change on NBP (Fig. 6.23). Strong positive effects were found in the Sahel and other parts of Africa, whereas negative effects were found in eastern and western Australia, and southwestern Europe (Fig. 6.23). Land cover and use changes drove NBP reductions in western South America, Sahel, and eastern Africa, along with slight increases in China and Eastern Europe (Fig. 6.23). All effects combined, the overall NBP trends were spatially variable, with strong positive trends in the central United States and eastern and southern Africa (Fig. 6.23). Although the influence of climate change on NBP was not significant (Fig. 6.22), it did explain a large proportion (72%) of

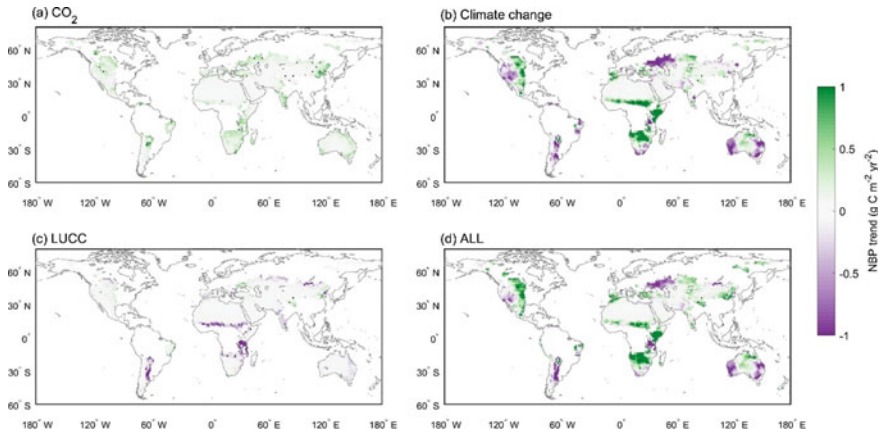


Fig. 6.23 Spatial patterns obtained by attribution analysis of NBP trends for 1980–2018. **a** CO₂-induced dryland NBP trends estimated from multiple DGVMs. **b** Climate change-induced NBP trends calculated from ensemble DGVMs. **c** Land cover and use change-induced NBP trends estimated from multiple DGVMs. **d** NBP trends simulated from multiple DGVMs. Stippling indicates pixels with a significant NBP trend ($p < 0.05$)

the variance in the spatial pattern of NBP, thus confirming the sensitivity of dryland ecosystems to climate change (Ahlström et al. 2015).

Increasing NBP trends were most pronounced in drylands in China ($9.75 \pm 7.63 \times 10^4 \text{ Pg C yr}^{-2}$), followed by the United States; both were dominated by the effect of CO₂ fertilization. Other areas showing increases included Botswana, Sudan, and Zambia, where drylands account for nearly 80% of the total land area of these countries. This trend was driven by climate change. Overall, climate change dominated the NBP trends in roughly two-thirds of dryland countries, whereas CO₂ fertilization and land cover and use changes dominated the trends in approximately 18% and 15% of all countries, respectively.

The ESM simulations provided by CMIP5 predict an increase in NBP in 2006–2100 in dryland ecosystems (under the RCP8.5 scenario), relative to 1986–2005, although there is a large interannual variation in these predictions (Fig. 6.24). Dryland NBP is predicted to increase from the beginning to middle of this century, followed by a decline toward the end of the century. Thus, annual mean NBP in drylands is expected to increase by $0.42 \pm 0.24 \text{ Pg C yr}^{-1}$ during 2081–2100, with the largest increase projected for western China (Fig. 6.24). Annual mean NBP is also predicted to increase in the northern hemisphere during this period, with simultaneous declines in the southern hemisphere. Under RCP8.5, carbon sinks in dryland ecosystems are expected to increase across 80% of the total global dryland area during 2081–2100.

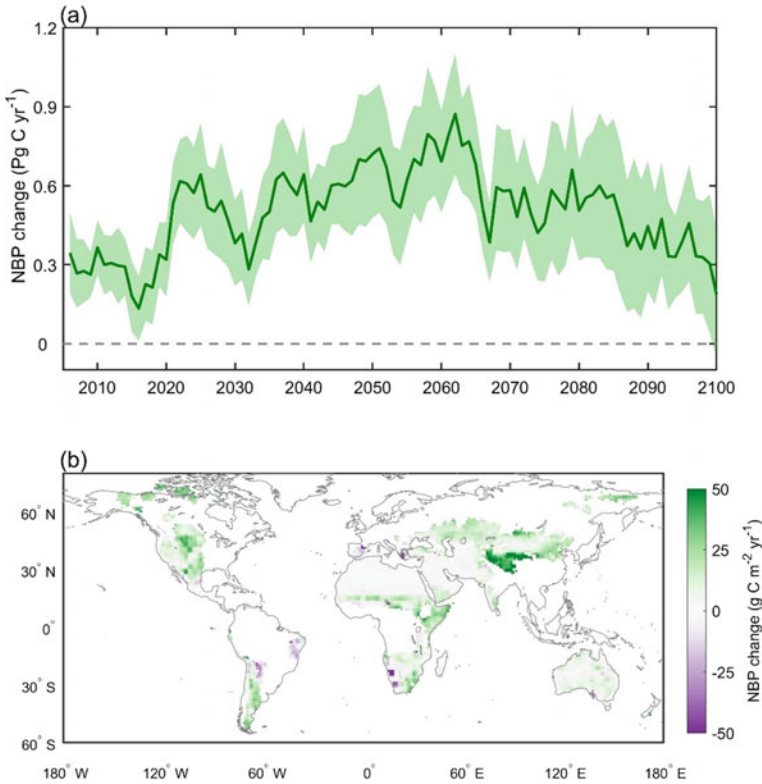


Fig. 6.24 Changes in annual mean NBP under RCP 8.5. **a** Temporal variation in NBP during 2006–2100 estimated using multiple ESMs in CMIP5. Data is smoothed using a 5-year running window. Shaded areas represent standard error among different ESMs. **b** NBP change predicted using multiple ESMs in CMIP5 during 2081–2100 relative to 1986–2005

6.3.3 Carbon–Water Coupling

The structure and function of vegetation in water-limited biomes are regulated by surface water availability and variations thereof. When plants open stomata to take up CO_2 for photosynthesis, they simultaneously lose water due to transpiration. This process links ecosystem carbon and water cycles. Plants can actively adjust the stomatal aperture to regulate the rates of photosynthesis and transpiration in response to changes in humidity, soil moisture, and atmospheric CO_2 concentration. This leads to changes in the WUE (carbon gained per unit of water lost) of vegetation.

Abundant evidence, provided by experimental and modeling studies, shows that plants can partially close stomata under higher atmospheric CO_2 concentrations, leading to higher leaf-level WUE (Cheng et al. 2017; Keenan et al. 2013; Knauer et al. 2017; Lee et al. 2011). For example, multi-year FACE experiments in semi-arid grasslands showed that elevated CO_2 concentration (>180 ppm above ambient CO_2

concentration) increased the rate of photosynthesis by 10% and decreased leaf stomatal conductance by 22%, translating to a 40% increase in leaf-level WUE (Lee et al. 2011). Greater WUE allows plants to reduce their water use while maintaining the same or increasing the rate of photosynthesis (Cheng et al. 2017). Climate change, particularly temperature-driven vapor-pressure deficits and precipitation-driven soil moisture changes, also affect WUE to some degree (Hatfield and Dold 2019). Recent evidence shows that under drought conditions, with low soil moisture and high vapor-pressure deficits, plants can maintain high WUE to alleviate extreme water stress (Peters et al. 2018). At the ecosystem level, WUE is often measured as the ratio of GPP to evapotranspiration (including transpiration, canopy interception, and bare soil evaporation) (Huang et al. 2015). In arid environments, those non-biological water fluxes (i.e., interception and soil evaporation) contribute substantially to evapotranspiration variations, responsive to changes in vegetation structure, such as an increase in leaf area. Therefore, leaf-level WUE variations may not scale to the ecosystem level.

According to the DGVMs, dryland ecosystem-level WUE increased significantly during 1980 – 2020, at an average rate of $0.039 \text{ g C m}^{-2} \text{ mm}^{-1} \text{ yr}^{-1}$ ($P < 0.05$; Fig. 6.25). Increased atmospheric CO_2 concentration is the primary driver of this increase, with a descending gradient from less to more extreme aridity (Fig. 6.25). This CO_2 -driven increase is slightly (~10%) offset by a decreasing trend caused by climate change. Unlike the positive effects of elevated CO_2 , climate change has significant negative effects on WUE in many dryland areas, including Australia, the western United States, South Africa, parts of northern China, Eastern Europe, and western Asia. Anthropogenic land use and management contributed little to the change in WUE during this period, although a decreasing trend in WUE was observed in the northern fringe of the Eurasian dryland area, i.e., the Mongolian steppe (Fig. 6.26). This regional decrease is at least partially attributable to grassland deterioration caused by overgrazing.

The ability to self-adjust water use efficiency is beneficial to the growth of vegetation. Stomatal regulation of transpiration under elevated CO_2 concentrations conserves water and reduces water limitations for photosynthesis and growth in arid and semi-arid ecosystems, known as the water-saving effect (Leuzinger and Körner 2007). C4 species benefit more than C3 species from CO_2 -induced water saving, as they show a stronger decline in stomatal conductance, allowing for greater increases in vegetation cover (Ainsworth and Rogers 2007; Morgan et al. 2011). Under global warming, the amount of conserved water is potentially sufficient for offsetting the higher water demands driven by a warmer atmosphere; this is likely the key mechanism underlying the enhanced carbon gains and increased biomass observed in dryland ecosystems (Lian et al. 2021). In drylands, the beneficial effects of increased CO_2 on vegetation growth through water saving is amplified by OF and processes including direct stimulation of photosynthesis (CO_2 fertilization effect) (Zhu et al. 2016), longer growing seasons (Hufkens et al. 2016), attenuated soil moisture stress in areas with increased precipitation (Al-Yaari et al. 2020), and human management activities (Chen et al. 2019).

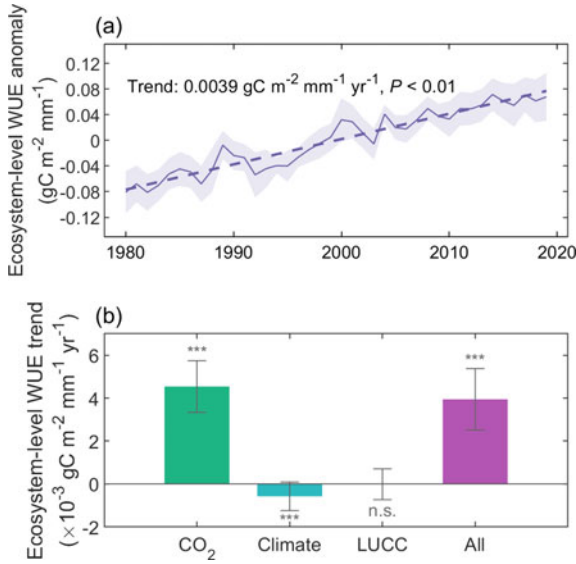


Fig. 6.25 Changes in ecosystem-level WUE in drylands during 1980–2018. **a** The solid line indicates the ensemble mean WUE of 14 DGVMs, with the shaded areas indicating standard deviations. Dashed lines indicate linear trends. **b** Trends in mean WUE attributed to elevated CO₂, climate change (Climate), and land cover change (LUC), based on DGVM factorial simulations. Error bars indicate standard deviations across models. ****p* < 0.01; ***p* < 0.05; **p* < 0.1; n.s., *p* > 0.1

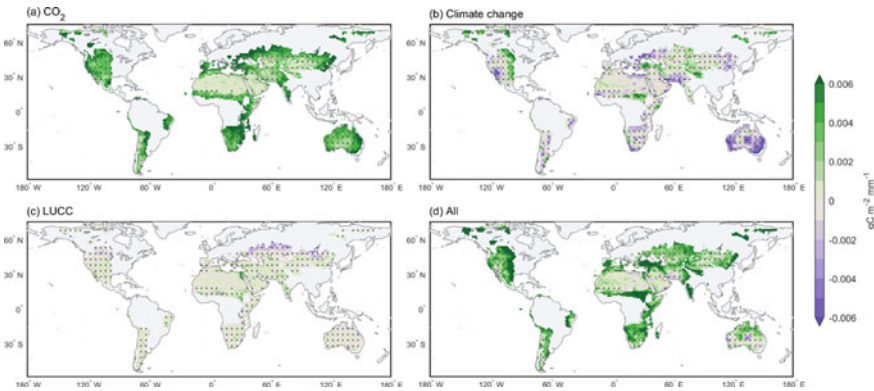


Fig. 6.26 Spatial patterns of the WUE trends for 1980–2019 over drylands, attributed to **a** elevated CO₂, **b** climate change, **c** land cover change (LUC), and **d** all factors combined. Changes were calculated using DGVM factorial simulations. Stippling indicates areas with statistically significant trends (*p* < 0.05)

6.4 Changes in Hydrological Regimes

In areas with scarce water resources, changes in water availability have profound impacts on ecosystem functions and services, including vegetation and agricultural productivity (Ciais et al. 2005; Gray et al. 2016), freshwater supplies (Greve et al. 2018), and ultimately the welfare of human societies. In recent years, the potential of exacerbating dryland water scarcity in drylands under climate change has gained widespread attention and led to extensive research (Feng and Fu 2013; Huang et al. 2016; Park et al. 2018; Zhang et al. 2020). A large number of studies use the aridity index which balances water received by the surface (precipitation) and that demanded by the atmosphere (potential evapotranspiration) as a proxy for assessing changes in land aridity (Feng and Fu 2013; Huang et al. 2016; Park et al. 2018). Under climate change, aridity index values tend to decrease because warming-induced increases in potential evapotranspiration outpace concurrent precipitation increases (Fu and Feng 2014; Huang et al. 2016; Sherwood and Fu 2014). More rapid increases in potential evapotranspiration are mainly attributed to an insufficient increase in actual water vapor relative to saturated water vapor which increases exponentially with temperature (i.e., higher vapor-pressure deficits). Therefore, assessments based on the aridity index are characterized by a broad trend of surface drying in global drylands, which translates to continuous expansion of the geographical extent of drylands. Climate model simulations under RCP 4.5 and RCP 8.5 indicate that climate change could lead to a 11–23% expansion in global dryland area by the end of the twenty-first century (Huang et al. 2017b, 2016).

A more comprehensive understanding of dryland aridity changes can be achieved by assessing hydrological metrics such as soil moisture, runoff, and terrestrial water storage (Lian et al. 2021; Roderick et al. 2015). Similar to atmospheric aridity metrics like the aridity index and vapor-pressure deficit, assessments based on soil moisture and runoff also indicate decreasing availability of freshwater resources over drylands. For example, station-recorded streamflow of the world's largest rivers flowing through drylands showed an overall decrease of 11.9% during 1948–2016 (Dai et al. 2009; Lian et al. 2021). Microwave satellite observations of near-surface soil moisture indicate that 38.4% of global drylands have shown a significant drying trend since 1979, whereas only 2.9% showed a wetting trend (Feng and Zhang 2015). For the period 2002–2016, gravimetric sensors onboard NASA's Gravity Recovery and Climate Experiment satellites indicated a robust decline in endorheic water storage, by 106.3 Gt yr⁻¹, mostly in global dryland areas (Wang et al. 2018).

Although surface water availability decreases following near-surface atmospheric drying, there is apparent divergence in long-term trends of water availability. A recent study evaluating water-stressed areas at the global scale used thresholds of various hydrological parameters and reported that the rate of dryland expansion inferred from soil moisture and runoff (i.e., the area under soil moisture and runoff deficits) was much smaller than that inferred from vapor-pressure deficits or the aridity index (Lian et al. 2021) (Fig. 6.27). This divergence indicates that although increased atmospheric evaporative demand would accelerate soil water depletion, this has not

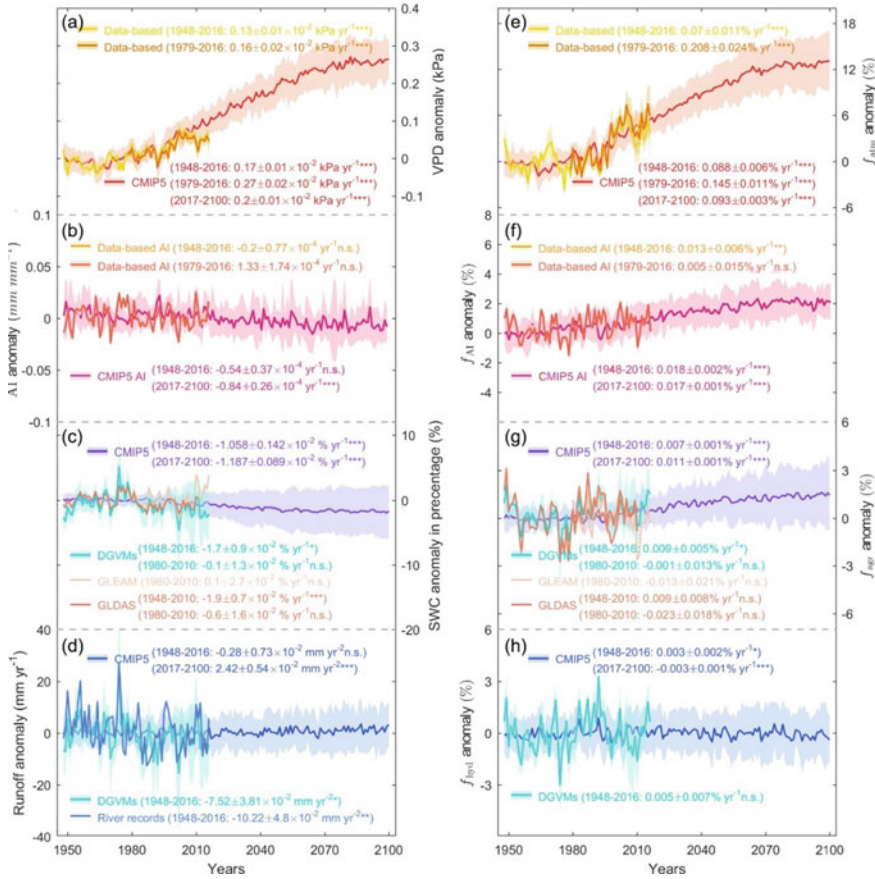


Fig. 6.27 Past and future dryland changes evaluated using different aridity measures including vapor-pressure deficit (VPD), aridity index (AI), soil water content (SWC), and runoff. This Fig. is based on the data used in Lian et al. (2021). **a–d** Various observational and model-derived anomalies in different aridity measures averaged over AI-defined baseline regions of drylands during 1961–1990. **e–h** Same as panels a–d, but showing anomalies (as %) in the fraction of water-stressed land areas (drylands) evaluated by these aridity measures. Shaded areas represent the 95% confidence intervals of multiple data sources (for VPD and AI) or model results (for DGVMs, or CMIP5 ESMs under ‘historical’ and ‘RCP 4.5’ scenarios)

fully translated into increased soil moisture and runoff deficits over drylands. Climate models also project persistence of the contemporary trend of soil drying to the end of the twenty-first century, but this is again less severe than that inferred from the projected atmospheric drying (Lian et al. 2021). However, projections under a warmer climate indicate that runoff increases may prevail in semi-arid and sub-humid dryland regions, although runoff decreases are projected for extremely arid regions (Lian et al. 2021).

The evolving ecosystem water consumption under climate change is thought to be a critical driver of the water available in soils and streams (Greve et al. 2014; Lian et al. 2021; Swann et al. 2016). In particular, plant physiological responses to higher CO₂ underlie the less severe surface drying trend than atmosphere-centered metrics. Stomatal regulation of transpiration under higher CO₂ favors the partitioning of precipitation towards runoff and soil moisture, thereby ameliorating the surface water losses driven by global warming (Greve et al. 2019; Scheff 2018; Swann et al. 2016). In future projections with, for example, quadrupled CO₂ from the pre-industrial level, modelling studies suggest that this CO₂ physiological forcing has a dominant effect on increased runoff production over CO₂ radiative forcing (Lian et al. 2021) (Fig. 6.28). Meanwhile, CO₂ physiological forcing substantially offsets radiative forcing-induced soil moisture decline (Lian et al. 2021; Swann et al. 2016). Although climate change dominates regional drying and wetting patterns, CO₂ physiological forcing acts to mitigate drying (or amplify wetting), particularly over some less arid dryland areas with sizeable vegetation cover (Fig. 6.29).

Although global patterns of aridification and dryland expansion remain debatable, there are clear regional hotspots of terrestrial water loss and increasing drought risks. For example, tree-ring reconstructions indicate an abrupt and unprecedented reduction in soil moisture during the twenty-first century in the western United States and interior East Asia, which overrides the range of natural variability of previous centuries (Williams et al. 2020; Zhang et al. 2020). This shift toward drier regimes is the result of a long-term precipitation deficit, and is further amplified and propagated through land–atmosphere coupling. Specifically, drier soils can suppress evaporative cooling and amplify increases in near-surface air temperature, which in turn amplifies soil moisture depletion (Seneviratne et al. 2010; Zhang et al. 2020). The

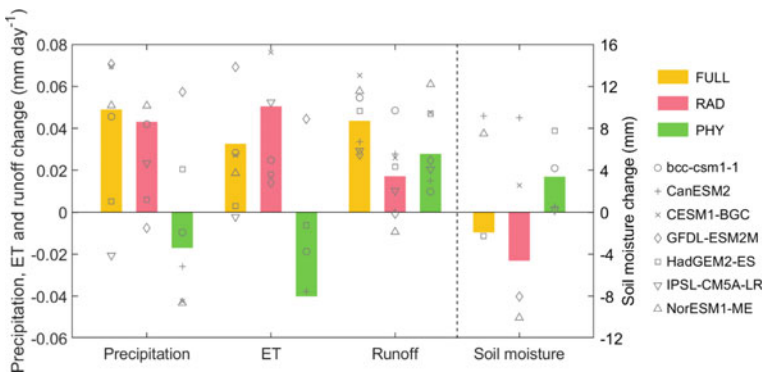


Fig. 6.28 Future changes in precipitation, evapotranspiration (ET), runoff, and soil moisture in global drylands. Bars (multi-model ensemble means) and symbols (individual models) show fractional changes in these variables caused by plant physiological responses to a quadrupling of atmospheric CO₂. Predictions are given for all CO₂-based forcings (FULL), and to physiological only forcings (PHY), and radiative only forcings (RAD). Changes were determined by subtracting the ensemble mean of the last 20 years from the first 20 years of seven CMIP5 models (bcc-csm1-1, CanESM2, CESM1-BGC, GFDL-ESM2M, HadGEM2-ES, IPSL-CM5A-LR, NorESM1-ME)

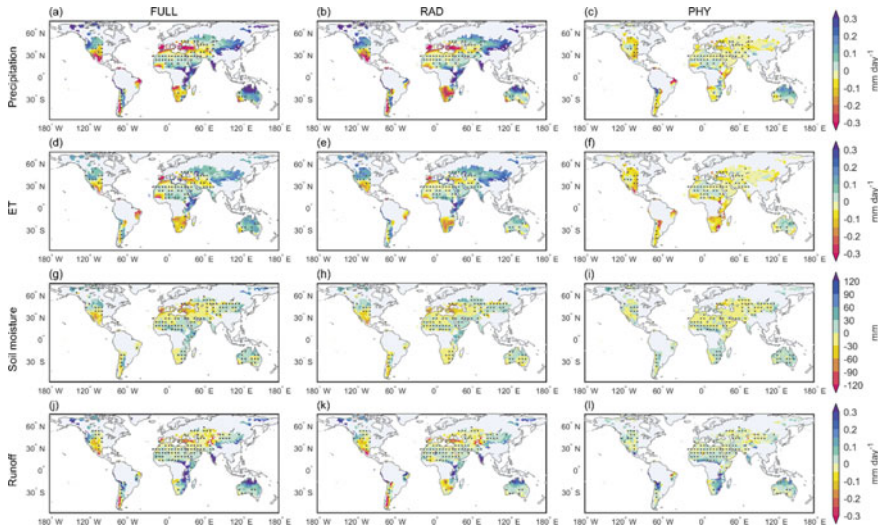


Fig. 6.29 Spatial patterns of future changes in **a–c** precipitation, **d–f** ET, **g–i** soil moisture, and **j–l** runoff from CMIP5 predictions. Columns represent predictions from all CO₂-based forcings (FULL), physiological only forcings (PHY), and radiative only forcings (RAD). Changes were determined by subtracting the ensemble mean of the last 20 years from the first 20 years of seven CMIP5 models (bcc-csm1-1, CanESM2, CESM1-BGC, GFDL-ESM2M, HadGEM2-ES, IPSL-CM5A-LR, NorESM1-ME). Dots indicate where at least five models agreed on the sign of the trend based on multi-model mean

unprecedented loss of water storage over some dryland regions is also the result of human activities such as afforestation, overgrazing, and agricultural expansion. For example, large-scale ecological restoration efforts in northern China have consumed an enormous amount of water and caused a decline in soil moisture (Feng et al. 2016; Zhao et al. 2020). These unintended hydrological consequences call for caution in additional reforestation programs in water-limited regions, where it is necessary to balance the benefits of forest ecosystem services with the costs of water resource consumption.

6.5 Vulnerability of Dryland Ecosystem and Human

6.5.1 Resistance and Resilience of Dryland Ecosystems

Drylands are among the most vulnerable ecosystems to anthropogenic climate change (IPCC 2019). Given the large predicted shifts in climate, especially warming (Huang et al. 2017a) and increased drought severity and frequency (Chiang et al. 2021), it is unclear how the stability of dryland ecosystem (i.e., the ability of ecosystem to

retain their functions under climatic perturbations) will change in a hotter and drier future.

The stability of a given ecosystem in response to external disturbance is generally assessed by two indices: resistance and resilience. Resistance represents the ability of vegetation to withstand disturbance, and is typically quantified as the magnitude of the reduction in vegetation growth or production during a disturbance event (Isbell et al. 2015; Lloret et al. 2011). Resilience represents the rate at which ecosystem functions return to their pre-disturbance state following an event (Gazol et al. 2018; Isbell et al. 2015), and has been defined as “the amount of disturbance a system can withstand before it crosses a threshold and fundamentally changes” (Ciemer et al. 2019; Liu et al. 2019; Scheffer et al. 2009; Verbesselt et al. 2016).

The resistance of dryland ecosystems to climate change varies among regions (Fig. 6.30) (Gazol et al. 2018). Low resistance to climate variation has been identified in the biomes of the prairies of North America, grasslands in Asia, and the Caatinga in Brazil (Seddon et al. 2016). These biomes have relatively high production, and are sensitive to variations of precipitation. On the contrary, biomes in the Sahel, Australian outback, and Middle East may be able to sustain relatively low but stable productivity despite large variability in precipitation, suggesting strong resistance to changes in water availability (Seddon et al. 2016).

The resilience of dryland ecosystem also varies widely across regions and biomes. Numerous evidence suggested that grassland production could fully recover or even overshoot within one year after droughts (Isbell, et al. 2015). Such rapid recovery could benefit from the compensate regrowth during rewetting events after droughts (Chen et al. 2020). In addition, grassland ecosystem has fast turnover rate in species composition. Drought events could lead to increasing abundance of drought-tolerate species, which also contributes to the rapid recovery in grasslands (Hoover et al. 2014). On the contrary, reduction of tree growth in forests under droughts could last for 1 to 4 years, and such drought “legacy effect” is especially pervasive in dry forests (Anderegg et al. 2015; Kannenberg et al. 2019). Vegetation growth rates are slow under harsh conditions in dry compared to humid regions, and these water-limited systems, therefore, take a long time to recover (Schwalm et al. 2017).

Some evidence suggests broad changes in ecosystem resistance and resilience over the past several decades, along with divergent response patterns among species (Anderegg et al. 2020; Fang and Zhang 2019; Gazol et al. 2018; Li et al. 2020). For example, an investigation of changes in resistance under repeated drought events showed decreased resistance among gymnosperm-dominated forests, but increasing resistance among angiosperm-dominated forests. This pattern of divergent behavior between gymnosperm and angiosperm species suggests that angiosperms may show stronger acclimation responses, whereas gymnosperms suffer greater stress accumulation (Anderegg et al. 2020). Whether forests are becoming more vulnerable to droughts depends not only on the changes of resistance during droughts, but also on the post-drought recovery. A recent study based on global tree-ring datasets showed a temporal trade-off between resistance and recovery in gymnosperm forests over the past six decades, with trees becoming more sensitive (decreased resistance), but recovering faster (increased resilience) during the post-drought period

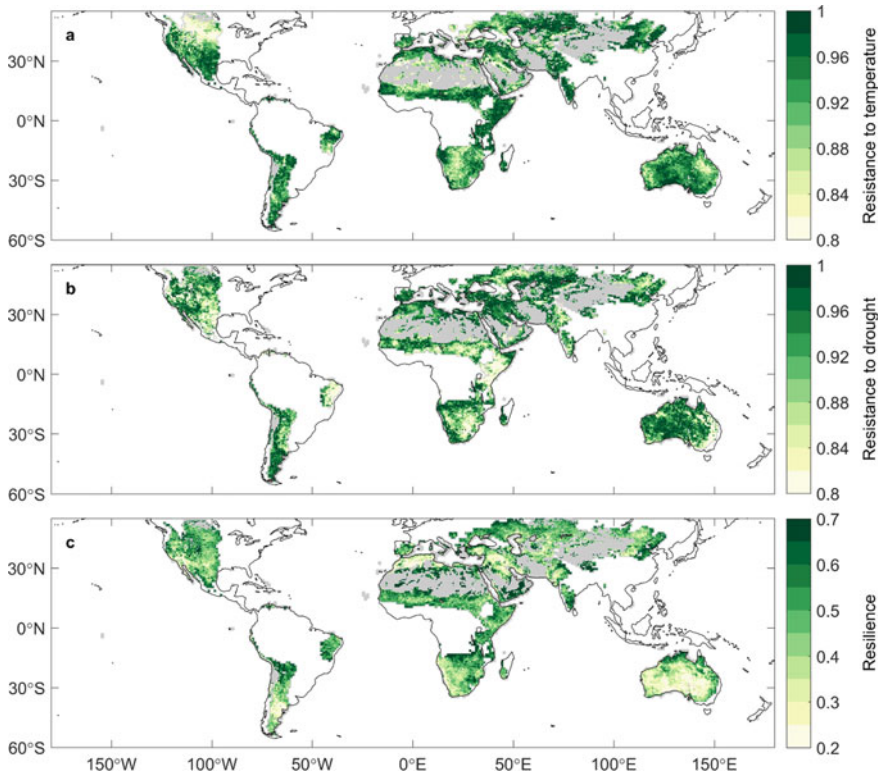


Fig. 6.30 Ecosystem resistance to **a** temperature and **b** drought, and **c** ecosystem resilience in drylands for the period 1982–2016. The resistance and resilience of ecosystem productivity (defined as the NDVI) were assessed based on the AR1 model ($NDVI_t = \alpha \times T + \beta \times SPEI + \gamma \times NDVI_{t-1} + \varepsilon$). Resistance was defined as 1 minus the absolute value of the model coefficient ($1-abs(\alpha)$ for temperature and $1-abs(\beta)$ for drought). Resilience was defined as 1 minus the absolute value of the model coefficient of $NDVI_{t-1}$ ($1-abs(\gamma)$). High values (shown in green) indicate strong resistance or resilience to climate change. Bare land areas ($NDVI < 0.1$) in dryland regions ($AI < 0.65$) are shown in grey

(Li et al. 2020). Enhanced post-drought recovery could be linked to the fertilization effect of an increased atmospheric CO_2 concentration, which would suggest that the rise in CO_2 may at least partly alleviate drought stress in gymnosperms (Li et al. 2020; Liu et al. 2017).

The hotter, drier climate of the future presents a threat to dryland ecosystems. The fate of these systems, i.e., whether they will adapt to the future climate or undergo degradation and desertification, remains controversial. For example, global warming and drought may increase mortality rates in forests and woodlands in dryland areas (Brodribb et al. 2020; Choat et al. 2018). However, an increased CO_2 concentration could increase WUE and to some extent enhance resilience to drought, potentially compensating for the damage caused by droughts and overall warming (Sperry et al.

2019). Moreover, our understanding of the types of tree species that may survive or perish under severe drought conditions remains limited. There is a pressing need to quantify the climate stress thresholds at which tree mortality and forest dieback occur, to develop mitigation strategies for dryland ecosystems under climate change (Trumbore et al. 2015).

6.5.2 Water Scarcity of the Dryland Socio-economic System

In drylands, the limited available surface water is a challenge for dryland countries to maintain sustainable food production and economic development. Based on climate model projections, surface freshwater resources (mainly runoff) in drylands will see an overall insignificant increase through the 21st Century, suggesting that the water supply to the socio-economic system is almost unchanged. However, the water scarcity conditions are determined by a balance between changes of water demand and water supply. Human water demand is the potential amount of water use by agricultural (livestock/irrigation), industrial (energy/manufacturing), and domestic sectors, related directly to human population and the level of economic development. Approximately 1/3 of the population living in drylands depends on agriculture for food and livelihoods, often as their only source of income, thus agriculture is the sector of the greatest anthropogenic water use.

The rates of human population growth and economic development in drylands are faster than the global average, driving simultaneously faster growing demand for freshwater. Based on global hydrological model simulations forced by historical and future socio-economic factors, human water demand in dryland countries has almost doubled since the 1950s (Fig. 6.31). This dryland water demand is projected to further increase by 270% towards the end of the twenty-first century in the absence of effective mitigation efforts (Fig. 6.31). The increasing anthropogenic use of water is also spatially imbalanced, which is more intense over developing than developed countries (Fig. 6.31). The water demand by Africa countries is projected to increase continuously in the next few decades, primarily contributed by agricultural expansion to meet growing food demands (Fig. 6.31). However, there will be a decline in water demand by North America and Australia after 2030s (Fig. 6.31), with adoption of efficient water management measures and water conservation technologies.

In many dryland areas, the rapidly growing anthropogenic water demand is likely to be a major driver of future water deficits in drylands. Local residents may excessively exploit river and groundwater resources to meet the increasing water demand. This unsustainable water consumption would induce less water resources available for dryland ecosystems, and increase the vulnerability of these already fragile ecosystems to climate change, which, in a feedback, ultimately jeopardize human societies. To ensure food security and cope with the increasing water crisis, more practical strategies are needed to develop more water-efficient technologies and improve the overall efficiency of water management.

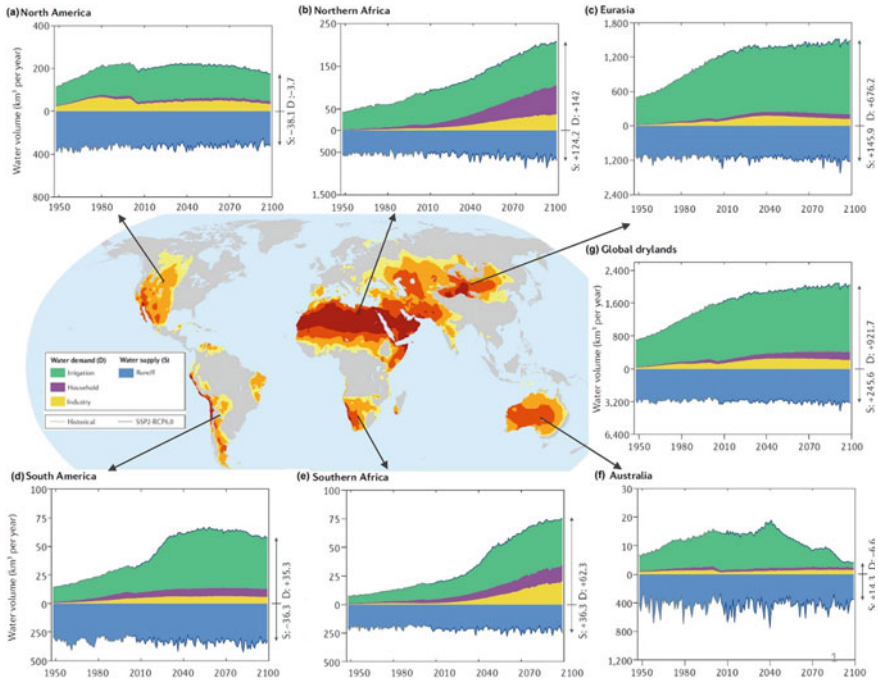


Fig. 6.31 Historical and future changes in total anthropogenic water use in global drylands. This figure is based on the data used in Lian et al. (2021). Water demand (D) is presented as the sum of agricultural, domestic, and industrial water withdrawal, and water supply (S) is primarily surface runoff. Note that the y-axis scale differs between D and S. The time series were derived from the ensemble mean of three global hydrological models (H08, MATSIRO and LPJmL) under the SSP2-RCP 6.0 scenario. Arrows indicate the amount of D and S during the 2090s, with the associated numbers showing relative changes from the 1961–1990 baseline

References

- Ahlström A, Raupach MR, Schurgers G et al (2015) The dominant role of semi-arid ecosystems in the trend and variability of the land CO_2 sink. *Science* 348(6237):895–899
- Ainsworth EA, Rogers A (2007) The response of photosynthesis and stomatal conductance to rising $[\text{CO}_2]$: mechanisms and environmental interactions. *Plant Cell Environ* 30(3):258–270
- Al-Yaari A, Wigneron J-P, Ciais P et al (2020) Asymmetric responses of ecosystem productivity to rainfall anomalies vary inversely with mean annual rainfall over the conterminous united states. *Glob Change Biol* 26(12):6959–6973
- Anav A, Friedlingstein P, Kidston M et al (2013) Evaluating the land and ocean components of the global carbon cycle in the cmip5 earth system models. *J Clim* 26(18):6801–6843
- Anderegg WR, Schwalm C, Biondi F et al (2015) Pervasive drought legacies in forest ecosystems and their implications for carbon cycle models. *Science* 349(6247):528–532
- Anderegg WRL, Trugman AT, Badgley G et al (2020) Divergent forest sensitivity to repeated extreme droughts. *Nat Clim Change* 10(12):1091–1095
- Badgley G, Field CB, Berry JA (2017) Canopy near-infrared reflectance and terrestrial photosynthesis. *Sci Adv* 3(3):e1602244

- Brodribb TJ, Powers J, Cochard H et al (2020) Hanging by a thread? Forests and drought. *Science* 368(6488):261–266
- Burrell AL, Evans JP, De Kauwe MG (2020) Anthropogenic climate change has driven over 5 million km² of drylands towards desertification. *Nat Commun* 11(1):3853
- Campbell JE, Berry JA, Seibt U et al (2017) Large historical growth in global terrestrial gross primary production. *Nature* 544(7648):84–87
- Challinor AJ, Watson J, Lobell DB (2014) A meta-analysis of crop yield under climate change and adaptation. *Nat Clim Change* 4(4):287–291
- Chazdon RL, Broadbent EN, Rozendaal DM et al (2016) Carbon sequestration potential of second-growth forest regeneration in the Latin American tropics. *Sci Adv* 2(5):e1501639
- Chen C, Park T, Wang X et al (2019) China and India lead in greening of the world through land-use management. *Nat Sustain* 2:122–129
- Chen N, Zhang Y, Zu J et al (2020) The compensation effects of post-drought regrowth on earlier drought loss across the tibetan plateau grasslands. *Agric for Meteorol* 281:107822
- Cheng L, Zhang L, Wang YP (2017) Recent increases in terrestrial carbon uptake at little cost to the water cycle. *Nat Commun* 8(1):110
- Chiang F, Mazdiyasn O, AghaKouchak A (2021) Evidence of anthropogenic impacts on global drought frequency, duration, and intensity. *Nat Commun* 12(1):2754
- Choat B, Brodribb TJ, Brodersen CR et al (2018) Triggers of tree mortality under drought. *Nature* 558(7711):531–539
- Ciais P, Reichstein M, Viovy N et al (2005) Europe-wide reduction in primary productivity caused by the heat and drought in 2003. *Nature* 437(7058):529–533
- Cierner C, Boers N, Hirota M et al (2019) Higher resilience to climatic disturbances in tropical vegetation exposed to more variable rainfall. *Nat Geosci* 12(3):174–179
- Dai A, Qian T, Trenberth KE et al (2009) Changes in continental freshwater discharge from 1948 to 2004. *J Clim* 22(10):2773–2792
- Donohue RJ, Roderick ML, McVicar TR et al (2013) Impact of CO₂ fertilization on maximum foliage cover across the globe's warm, arid environments. *Geophys Res Lett* 40(12):3031–3035
- Drake BG, Leadley PW, Arp WJ et al (1989) An open top chamber for field studies of elevated atmospheric CO₂ concentration on saltmarsh vegetation. *Funct Ecol* 3:363–371
- Fang O, Zhang QB (2019) Tree resilience to drought increases in the tibetan plateau. *Glob Change Biol* 25(1):245–253
- Feng S, Fu Q (2013) Expansion of global drylands under a warming climate. *Atmos Chem Phys Discuss* 13(6):14637–14665
- Feng H, Zhang M (2015) Global land moisture trends: drier in dry and wetter in wet over land. *Sci Rep* 5(1):18018
- Feng X, Fu B, Piao S et al (2016) Revegetation in china's loess plateau is approaching sustainable water resource limits. *Nat Clim Change* 6(11):1019–1022
- Foley JA, DeFries R, Asner GP et al (2005) Global consequences of land use. *Science* 309(5734):570–574
- Fu Q, Feng S (2014) Responses of terrestrial aridity to global warming. *J Geophys Res Atmos* 119(13):7863–7875
- Gazol A, Camarero JJ, Vicente-Serrano SM et al (2018) Forest resilience to drought varies across biomes. *Glob Change Biol* 24(5):2143–2158
- Gonsamo A, Ciais P, Miralles DG et al (2021) Greening drylands despite warming consistent with carbon dioxide fertilization effect. *Glob Change Biol* 27(14):3336–3349
- Gray SB, Dermody O, Klein SP et al (2016) Intensifying drought eliminates the expected benefits of elevated carbon dioxide for soybean. *Nat Plants* 2(9):16132
- Greve P, Orlovsky B, Mueller B et al (2014) Global assessment of trends in wetting and drying over land. *Nat Geosci* 7(10):716–721
- Greve P, Kahil T, Mochizuki J et al (2018) Global assessment of water challenges under uncertainty in water scarcity projections. *Nat Sustain* 1(9):486–494

- Greve P, Roderick ML, Ukkola AM et al (2019) The aridity index under global warming. *Environ Res Lett* 14(12):124006
- Hansen MC, Potapov PV, Moore R et al (2013) High-resolution global maps of 21st-century forest cover change. *Science* 342(6160):850–853
- Hatfield JL, Dold C (2019) Water-use efficiency: advances and challenges in a changing climate. *Front Plant Sci* 10:103
- Hoover DL, Knapp AK, Smith MD (2014) Resistance and resilience of a grassland ecosystem to climate extremes. *Ecology* 95(9):2646–2656
- Hovenden MJ, Leuzinger S, Newton PC et al (2019) Globally consistent influences of seasonal precipitation limit grassland biomass response to elevated CO₂. *Nat Plants* 5(2):167–173
- Huang M, Piao S, Sun Y et al (2015) Change in terrestrial ecosystem water-use efficiency over the last three decades. *Glob Change Biol* 21(6):2366–2378
- Huang J, Yu H, Guan X et al (2016) Accelerated dryland expansion under climate change. *Nat Clim Change* 6(2):166–171
- Huang J, Li Y, Fu C et al (2017a) Dryland climate change: recent progress and challenges. *Rev Geophys* 55(3):719–778
- Huang J, Yu H, Dai A et al (2017b) Drylands face potential threat under 2°C global warming target. *Nat Clim Change* 7(6):417–422
- Huete A, Didan K, Miura T et al (2002) Overview of the radiometric and biophysical performance of the Modis vegetation indices. *Remote Sens Environ* 83(1–2):195–213
- Hufkens K, Keenan TF, Flanagan LB et al (2016) Productivity of north american grasslands is increased under future climate scenarios despite rising aridity. *Nat Clim Change* 6(7):710–714
- Iizumi T, Sakai T (2020) The global dataset of historical yields for major crops 1981–2016. *Sci Data* 7(1):1–7
- IPCC (2019) Climate change and land: An ipcc special report on climate change, desertification, land degradation, sustainable land management, food security, and greenhouse gas fluxes in terrestrial ecosystems. In: Shukla P, Skea J, Calvo Buendia E et al (ed)
- Isbell F, Craven D, Connolly J et al (2015) Biodiversity increases the resistance of ecosystem productivity to climate extremes. *Nature* 526(7574):574–577
- Jiang C, Ryu Y, Fang H et al (2017) Inconsistencies of interannual variability and trends in long-term satellite leaf area index products. *Glob Change Biol* 23(10):4133–4146
- Jung M, Schwalm C, Migliavacca M et al (2020) Scaling carbon fluxes from eddy covariance sites to globe: synthesis and evaluation of the fluxcom approach. *Biogeosciences* 17(5):1343–1365
- Kannenberg SA, Novick KA, Alexander MR et al (2019) Linking drought legacy effects across scales: from leaves to tree rings to ecosystems. *Glob Change Biol* 25(9):2978–2992
- Kantzas E, Quegan S, Lomas M (2015) Improving the representation of fire disturbance in dynamic vegetation models by assimilating satellite data: a case study over the arctic. *Geosci Model Dev* 8(8):2597–2609
- Keenan TF, Riley WJ (2018) Greening of the land surface in the world's cold regions consistent with recent warming. *Nat Clim Change* 8:825–828
- Keenan TF, Hollinger DY, Bohrer G et al (2013) Increase in forest water-use efficiency as atmospheric carbon dioxide concentrations rise. *Nature* 499(7458):324–327
- Knauer J, Zaehle S, Reichstein M et al (2017) The response of ecosystem water-use efficiency to rising atmospheric CO₂ concentrations: sensitivity and large-scale biogeochemical implications. *New Phytol* 213(4):1654–1666
- Kummu M, Taka M, Guillaume JHA (2018) Gridded global datasets for gross domestic product and human development index over 1990–2015. *Sci Data* 5(1):180004
- Le Quéré C, Raupach MR, Canadell JG et al (2009) Trends in the sources and sinks of carbon dioxide. *Nat Geosci* 2(12):831–836
- Leadley PW, Drake BG (1993) Open top chambers for exposing plant canopies to elevated CO₂ concentration and for measuring net gas exchange CO₂ and biosphere. Springer, pp 3–16

- Lee TD, Barrott SH, Reich PB (2011) Photosynthetic responses of 13 grassland species across 11 years of free-air CO₂ enrichment is modest, consistent and independent of N supply. *Glob Change Biol* 17(9):2893–2904
- Leuzinger S, Körner C (2007) Water savings in mature deciduous forest trees under elevated CO₂. *Glob Change Biol* 13(12):2498–2508
- Li Y, Kalnay E, Motesharrei S et al (2018) Climate model shows large-scale wind and solar farms in the Sahara increase rain and vegetation. *Science* 361(6406):1019–1022
- Li X, Piao S, Wang K, Wang X et al (2020) Temporal trade-off between gymnosperm resistance and resilience increases forest sensitivity to extreme drought. *Nat Ecol Evol* 4:1075–1083
- Lian X, Piao S, Chen A et al (2021) Multifaceted characteristics of dryland aridity changes in a warming world. *Nat Rev Earth Environ* 2:232–250
- Liu Y, Parolari AJ, Kumar M et al (2017) Increasing atmospheric humidity and CO₂ concentration alleviate forest mortality risk. *Proc Natl Acad Sci USA* 114(37):9918–9923
- Liu Y, Kumar M, Katul GG et al (2019) Reduced resilience as an early warning signal of forest mortality. *Nat Clim Change* 9(11):880–885
- Liu Y, Liu R, Chen JM (2012) Retrospective retrieval of long-term consistent global leaf area index (1981–2011) from combined AVHRR and MODIS data. *J Geophys Res Biogeosci* 117:G04003
- Lloret F, Keeling EG, Sala A (2011) Components of tree resilience: effects of successive low-growth episodes in old ponderosa pine forests. *Oikos* 120(12):1909–1920
- Morgan JA, LeCain DR, Pendall E et al (2011) C₄ grasses prosper as carbon dioxide eliminates desiccation in warmed semi-arid grassland. *Nature* 476(7359):202–205
- Murray-Tortarolo G, Anav A, Friedlingstein P et al (2013) Evaluation of land surface models in reproducing satellite-derived LAI over the high-latitude northern hemisphere. Part I: uncoupled DgvmS. *Remote Sens* 5(10):4819–4838
- Myneni RB, Hoffman S, Knyazikhin Y et al (2002) Global products of vegetation leaf area and fraction absorbed PAR from year one of MODIS data. *Remote Sens Environ* 83(1–2):214–231
- Neumann K, Sietz D, Hilderink H et al (2015) Environmental drivers of human migration in drylands—a spatial picture. *Appl Geogr* 56:116–126
- Norby RJ, Zak DR (2011) Ecological lessons from free-air CO₂ enrichment (FACE) experiments. *Annu Rev Ecol Syst* 42(1):181–203
- Norby RJ, Warren JM, Iversen CM et al (2010) CO₂ enhancement of forest productivity constrained by limited nitrogen availability. *Proc Natl Acad Sci USA* 107(45):19368–19373
- Pan Y, Birdsey RA, Fang J et al (2011) A large and persistent carbon sink in the world's forests. *Science* 333(6045):988–993
- Park C-E, Jeong S-J, Joshi M et al (2018) Keeping global warming within 1.5 °C constrains emergence of aridification. *Nat Clim Change* 8(1):70–74
- Peters W, van der Velde IR, van Schaik E et al (2018) Increased water-use efficiency and reduced CO₂ uptake by plants during droughts at a continental-scale. *Nat Geosci* 11(9):744–748
- Piao S, Fang J, Ciais P et al (2009) The carbon balance of terrestrial ecosystems in China. *Nature* 458(7241):1009–1013
- Piao S, Huang M, Liu Z et al (2018) Lower land-use emissions responsible for increased net land carbon sink during the slow warming period. *Nat Geosci* 11(10):739–743
- Piao S, Wang X, Park T et al (2020) Characteristics, drivers and feedbacks of global greening. *Nat Rev Earth Environ* 1(1):14–27
- Pinzon J, Tucker C (2014) A non-stationary 1981–2012 AVHRR NDVI3g time series. *Remote Sens* 6(8):6929–6960
- Poulter B, Frank D, Ciais P et al (2014) Contribution of semi-arid ecosystems to interannual variability of the global carbon cycle. *Nature* 509(7502):600–603
- Reich PB, Hobbie SE, Lee TD (2014) Plant growth enhancement by elevated CO₂ eliminated by joint water and nitrogen limitation. *Nat Geosci* 7(12):920–924
- Roderick ML, Greve P, Farquhar GD (2015) On the assessment of aridity with changes in atmospheric CO₂. *Water Resour Res* 51(7):5450–5463

- Rosenzweig C, Jones JW, Hatfield JL et al (2013) The agricultural model intercomparison and improvement project (agmip): Protocols and pilot studies. *Agric for Meteorol* 170:166–182
- Scheff J (2018) Drought indices, drought impacts, CO₂, and warming: a historical and geologic perspective. *Curr Clim Chang Rep* 4(2):202–209
- Scheffer M, Bascompte J, Brock WA et al (2009) Early-warning signals for critical transitions. *Nature* 461(7260):53–59
- Schwalm CR, Anderegg WRL, Michalak AM et al (2017) Global patterns of drought recovery. *Nature* 548(7666):202–205
- Seddon AW, Macias-Fauria M, Long PR et al (2016) Sensitivity of global terrestrial ecosystems to climate variability. *Nature* 531(7593):229–232
- Seneviratne SI, Corti T, Davin EL et al (2010) Investigating soil moisture–climate interactions in a changing climate: a review. *Earth-Science Rev* 99(3–4):125–161
- Sherwood S, Fu Q (2014) A drier future? *Science* 343(6172):737–739
- Sitch S, Friedlingstein P, Gruber N et al (2015) Recent trends and drivers of regional sources and sinks of carbon dioxide. *Biogeosciences* 12(3):653–679
- Smith WK, Dannenberg MP, Yan D et al (2019) Remote sensing of dryland ecosystem structure and function: progress, challenges, and opportunities. *Remote Sens Environ* 233:111401
- Song XP, Hansen MC, Stehman SV et al (2018) Global land change from 1982 to 2016. *Nature* 560(7720):639–643
- Sperry JS, Venturas MD, Todd HN et al (2019) The impact of rising CO₂ and acclimation on the response of us forests to global warming. *Proc Natl Acad Sci USA* 116(51):25734–25744
- Swann AL, Hoffman FM, Koven CD et al (2016) Plant responses to increasing CO₂ reduce estimates of climate impacts on drought severity. *Proc Natl Acad Sci USA* 113(36):10019–10024
- Terrer C, Vicca S, Hungate BA et al (2016) Mycorrhizal association as a primary control of the CO₂ fertilization effect. *Science* 353(6294):72–74
- Tian S, Van Dijk AIJM, Tregoney P et al (2019) Forecasting dryland vegetation condition months in advance through satellite data assimilation. *Nat Commun* 10:469
- Tilman D, Balzer C, Hill J et al (2011) Global food demand and the sustainable intensification of agriculture. *Proc Natl Acad Sci USA* 108(50):20260–20264
- Trumbore S, Brando P, Hartmann H (2015) Forest health and global change. *Science* 349(6250):814–818
- Ukkola AM, De Kauwe MG, Roderick ML et al (2021) Annual precipitation explains variability in dryland vegetation greenness globally but not locally. *Glob Change Biol* 27(18):4367–4380
- Verbesselt J, Umlauf N, Hirota M et al (2016) Remotely sensed resilience of tropical forests. *Nat Clim Change* 6(11):1028–1031
- Wang W, Dungan J, Hashimoto H et al (2011) Diagnosing and assessing uncertainties of terrestrial ecosystem models in a multimodel ensemble experiment: 1 Primary production. *Glob Change Biol* 17(3):1350–1366
- Wang J, Song C, Reager JT et al (2018) Recent global decline in endorheic basin water storages. *Nat Geosci* 11:926–932
- Warszawski L, Frieler K, Huber V et al (2014) The inter-sectoral impact model intercomparison project (isi-mip): project framework. *Proc Natl Acad Sci USA* 111(9):3228–3232
- Welp LR, Keeling RF, Meijer HAJ et al (2011) Interannual variability in the oxygen isotopes of atmospheric CO₂ driven by el niño. *Nature* 477(7366):579–582
- Williams AP, Cook ER, Smerdon JE et al (2020) Large contribution from anthropogenic warming to an emerging North American megadrought. *Science* 368(6488):314–318
- Xu L, Myneni RB, Chapin III FS et al (2013) Temperature and vegetation seasonality diminishment over northern lands. *Nat Clim Change* 3(6):581–586
- Yan K, Park T, Yan G et al (2016) Evaluation of modis L3/4P product collection 6 Part 1: consistency and improvements. *Remote Sensing* 8(5):359
- Yuan W, Zheng Y, Piao S, et al (2019) Increased atmospheric vapor pressure deficit reduces global vegetation growth. *Sci Adv* 5(8):eaax1396

- Zelnik YR, Kinast S, Yizhaq H et al (2013) Regime shifts in models of dryland vegetation. *Philos Trans R Soc A Math Phys Eng Sci* 371:20120358
- Zhang Y, Song C, Band LE et al (2017) Reanalysis of global terrestrial vegetation trends from Modis products: browning or greening? *Remote Sens Environ* 191:145–155
- Zhang Y, Joiner J, Alemohammad SH et al (2018) A global spatially contiguous solar-induced fluorescence (CSIF) dataset using neural networks. *Biogeosciences* 15(19):5779–5800
- Zhang P, Jeong J-H, Yoon J-H et al (2020) Abrupt shift to hotter and drier climate over inner East Asia beyond the tipping point. *Science* 370(6520):1095–1099
- Zhao C, Piao S, Huang Y et al (2016) Field warming experiments shed light on the wheat yield response to temperature in China. *Nat Commun* 7:13530
- Zhao M, Geruo A, Zhang J et al (2020) Ecological restoration impact on total terrestrial water storage. *Nat Sustain* 4:56–62
- Zhou T, Shi P, Jia G et al (2015) Age-dependent forest carbon sink: estimation via inverse modeling. *J Geophys Res Biogeosci* 120(12):2473–2492
- Zhu Z, Bi J, Pan Y et al (2013) Global data sets of vegetation leaf area index (lai)3g and fraction of photosynthetically active radiation (fpar)3g derived from global inventory modeling and mapping studies (gimms) normalized difference vegetation index (ndvi3g) for the period 1981 to 2011. *Remote Sens* 5(2):927–948
- Zhu Z, Piao S, Myneni RB et al (2016) Greening of the earth and its drivers. *Nat Clim Change* 6(8):791–795
- Zhu Z, Piao S, Lian X et al (2017) Attribution of seasonal leaf area index trends in the northern latitudes with “optimally” integrated ecosystem models. *Glob Change Biol* 23(11):4798–4813

Open Access This chapter is licensed under the terms of the Creative Commons Attribution 4.0 International License (<http://creativecommons.org/licenses/by/4.0/>), which permits use, sharing, adaptation, distribution and reproduction in any medium or format, as long as you give appropriate credit to the original author(s) and the source, provide a link to the Creative Commons license and indicate if changes were made.

The images or other third party material in this chapter are included in the chapter’s Creative Commons license, unless indicated otherwise in a credit line to the material. If material is not included in the chapter’s Creative Commons license and your intended use is not permitted by statutory regulation or exceeds the permitted use, you will need to obtain permission directly from the copyright holder.

